12-8-2023

Modeling compound effects of earthquakes and flooding on the failure probability of earthen levees

Mohammad Reza Mahdavizadeh
Mohammad Reza Mahdavizadeh, mm4893@msstate.edu

Modeling compound effects of earthquakes and flooding

on the failure probability of earthen levees

By

Mohammad Reza Mahdavizadeh

Approved by:

Farshid Vahedifard (Major Professor/Graduate Coordinator)
Jeremiah M. Stache
Seamus Freyne
Jason M. Keith (Dean, Bagley College of Engineering)

A Thesis
Submitted to the Faculty of
Mississippi State University
in Partial Fulfillment of the Requirements
for the Degree of Master of Science
in Civil Engineering
in the Richard A. Rula School of Civil and Environmental Engineering

Mississippi State, Mississippi

December 2023

Name: Mohammad Reza Mahdavizadeh

Date of Degree: December 8, 2023

Institution: Mississippi State University

Major Field: Civil Engineering

Major Professor: Farshid Vahedifard

Title of Study: Modeling compound effects of earthquakes and flooding on the failure probability of earthen levees

Pages in Study: 65

Candidate for Degree of Master of Science

Earthen levees are crucial components of a nation's flood protection system. However, in some regions, these levees face the unique challenge of being subjected to both floods and earthquakes throughout their lifespan, an aspect that is relatively unexplored in the existing literature. The primary aim of this research is to examine earthquakes' and floods' effects on earthen levee failures. Using numerical simulations, the seepage, slope stability, and liquefaction potential of an earthen levee were modeled by considering compound of different floods and earthquakes scenarios. Elkhorn Levee in Sacramento, CA, was used as a representative case study for the simulations. The probability of levee failure and the extent of the breach caused by compound flood-earthquake scenarios are further determined by Fault Tree Method. The findings provide a practical approach to analyzing levee systems under multi-hazard conditions and enhancing levee resilience.

DEDICATION

To my wife Anahita Pirzad. I would like to thank you for your tremendous patience, love, and support throughout my education journey. I am sure, this one year was so difficult for you, but I am happy that we were able to achieve this goal together.

ACKNOWLEDGEMENTS

It would be my pleasure to express my deepest gratitude to my advisor, Dr. Farshid Vahedifard, for his support and guidance throughout my educational journey. Throughout my journey, Dr. Vahedifard has consistently pushed me to reach my full potential, providing me with a constant source of support and encouragement along the way. Thank you for providing me with the guidance, friendship, and financial assistance that you diligently secured on my behalf. Your unwavering support has contributed to my academic and personal development, and I am very grateful for the opportunities you have provided me. Additionally, I would like to express my sincere gratitude to the members of my committee. Jeremiah M. Stache: I appreciate the patience and willingness with which you explained complex concepts during the courses we had together. My understanding of geotechnical principles and practices was greatly enhanced by your teachings. Dr. Seamus Freyne: I would like to express my gratitude for accepting to be a member of my committee. It is a pleasure to receive your valuable review and feedback on my research.

Lastly, I want to thank all of my colleagues for their support and companionship. Thank you, Dr. Mohsen Ajdari, Mohammad Azhar and Amirali Asadian.

TABLE OF CONTENTS

LIST OF TABLES

LIST OF FIGURES

CHAPTER I

INTRODUCTION AND BACKGROUND

Introduction and Background

Earthen levees are crucial components of the nation's flood protection system, playing a vital role in safeguarding communities against flooding events (Kundzewicz 1999). However, in several regions, these levees face the unique challenge of being subjected to the compound effects of floods and earthquakes throughout their lifespan, an aspect that remains relatively unexplored in the existing literature. Levees are vital structures designed to protect low land from flooding, including riverside towns, agricultural areas, and urban developments (Miguez et al. 2015). When an earthquake strikes, these structures can be subjected to various hazards that compromise their integrity and functionality (Deverel et al. 2016). This can result in breaching or failure during subsequent flood events, leading to extensive flooding, property damage, and destruction of homes and infrastructure.

Earthquakes may damage levees through different mechanisms. Firstly, the ground shaking caused by seismic waves can lead to liquefaction. Liquefaction occurs when the soil beneath the levee loses its strength and stiffness, turning into a liquid-like state (Huang and Yu 2013). This weakens the foundation of the levee, making it more susceptible to failure. Secondly, an earthquake can trigger landslides or slope failures along the levee's embankments (Duncan et al. 2014). The rapid movement of soil and rock can damage or weaken the structure, compromising its ability to hold back water effectively. Additionally, the dynamic forces from the earthquake can

induce differential settlement in the levee, causing it to tilt or deform. Such deformation can create weak points and increase the risk of damage during subsequent flood events (Alexander 2018). Furthermore, seismic activity can cause fractures or cracks in the levee's core material or protective layers. These cracks can provide pathways for water infiltration, weakening the structure over time and making it more vulnerable to flooding (Robinson and Vahedifard 2016).

Over the past few decades, numerous research has been carried out to gain a better understanding of soil dynamics and its underlying mechanisms. These researches aimed to provide valuable insights into the hydro-dynamic behavior of geo-structures like levees (Seed and Idriss 1971; Poulos et al. 1985; Ishihara 1993; Toprak and Holzer 2003; Jefferies and Been 2015; Selmi et al. 2022). While these previous studies have made significant advancements, it is important to note that the potential impact of simultaneous flood and earthquake events on the safety of levees has received limited, if any, attention.

Objectives

The primary objective of this research is to investigate the compound effect of earthquakes and flooding on the failure probability of earthen levees. To achieve this goal, a comprehensive set of numerical simulations was conducted to model seepage, slope stability, and liquefaction potential in an earthen levee under the influence of flood and earthquake events. The simulations were specifically performed on the Elkhorn Levee in Sacramento, CA, as a representative case study. This area is at a high risk of natural disasters due to its dense population, numerous levees, and various reasons for potential levee failure, such as earthquakes, heavy rains, and poor maintenance. The Sacramento-San Joaquin Delta covers about 738,000 acres of mostly rural land, and it relies on a network of 1,800 kilometers of levees that span its entire length to protect it from potential disasters (Flynn 2007; Abdollahi et al. 2021). Sacramento has relatively low levels of

natural hazards as compared with other cities in the state. There are a number of factors that contribute to this favorable status, including the low seismic activity history of the region. Due to this, the probability of a ground motion causing various levels of discomfort in Sacramento is generally lower than that of other areas in the country (Burton and Cutter 2008). However, it is crucial to recognize that no region in California can completely dismiss the possibility of future earthquakes. Despite experiencing lower hazard levels, Sacramento is still at risk of experiencing significant ground motions (USGS 2022).

Scope and Contribution

To achieve the given objectives, we used the GeoStudio commercially available software package, which includes SEEP/W, SLOPE/W, SIGMA/W, and QUAKE/W modules to model the Elkhorn levee in Sacramento County, California under the compound influence of floods and seismic loading.

For different flood scenarios, we used the flood level of water for different recurrence intervals using the historical (1950-2000) and projected future (2049-2099) simulations which are presented by Vahedifard et al. (2020). Two different flood duration scenarios were applied to the levee based on the elevation of the water level behind the upstream side. For the first scenario, the elevation of the water level is regulated so that the normal water level is reached at the end of the flood time duration. For the second scenario, several models were developed to simulate the rapid drawdown phenomenon afterward the phreatic line reaches its steady state.

In this study, we used the Kern County earthquake time history which occurred on July 21, 1952, with the magnitude of 7.3 and peak ground acceleration of approximately 0.16g, in the southern San Joaquin Valley, to apply it as the seismic loading at the base of the levee's foundation. In this study, we analyzed various earthquake scenarios for the Sacramento region by considering

four different earthquakes return periods coincided by six different floods. The maximum peak ground acceleration values for each scenario were obtained from the research conducted by USGS (2022). Additionally, we modified the time history data of the 1952 Kern County earthquake by adjusting it to match the new peak ground acceleration values obtained from Chowdhury's research. This allowed us to study the potential effects of different earthquake intensities on the Sacramento region.

Different analysis methods were employed during our modeling process. Simulating steady-state and transient flows was accomplished using SEEP/W. Prior to the earthquake, SIGMA/W was used to establish the initial static stress state. QUAKE/W was used to apply seismic loads to the levee, and SLOPE/W was used to assess slope stability before and after the seismic event. The permanent deformation resulting from the earthquake was also estimated using QUAKE/W Newmark Deformation.

The Fault Tree Method is further used to determine the reliability of the levee by considering the probability of coincidental floods and earthquakes occurring subsequently. As a result, this contributes to the development of updated risk assessments for geo-structures in areas of high risk.

CHAPTER II

LITERATURE REVIEW

Introduction

As a consequence of global warming caused by human activities, heavy rainfall events are becoming more frequent all over the world (Swain et al. 2020). Recent evidence has increasingly supported the claim, with an observed escalation in heavy precipitation events in the United States (Wright et al. 2019). Specifically, seasonal rivers, characterized by their long and narrow pathways, are one of the primary contributors to the extreme floods that take place in California (Huang et al. 2020). Several major reservoirs have been exposed to high-risk situations as a result of the flooding occurring in California in 2017. This flooding resulted in over 85% of the reservoirs being overfilled, posing some threats to the facilities. (Mallakpour et al. 2020; Abdollahi and Vahedifard 2021).

Human-made structures such as levees and earthen embankment dams play a crucial role in flood control during heavy rainfall and when the water level is high (Zimmaro et al. 2019). Conversely, these geo-structures are often constructed in seismic zones and are subjected to dynamic loading from earthquakes, resulting in various forms of instability like liquefaction, slope instability, ground rupture, and excessive permanent deformation. (Wu et al. 2021). Intense seismic shaking induces shear stresses and strains within a slope, which may surpass the strength and stability thresholds of the slope materials, and consequently result in slope failure and subsequent landslides. Seismic shaking induces shearing forces within embankments, leading to

the development of shear strains. Once these strains exceed the elastic limit of the embankment material, permanent settlements occur. The progressive accumulation of shear strains can ultimately lead to shear failure or substantial deformations. To prevent various kinds of damage from quakes, it is vital to carefully design, construct, and maintain these structures (Franczyk et al. 2016; Mallakpour et al. 2020; Abdollahi and Vahedifard 2020). In this chapter, studies available in the literature dealing with the behavior of soil embankments under compound hydraulic and dynamic loadings as well as numerical analytical methods related to these kinds of analysis are reviewed.

Levees under Cascading Hazards

Multi-hazard risk analysis is a complex and challenging procedure that involves assessing and analyzing the compound effects of multiple hazards on a system or region (Eshrati et al. 2015). Unlike single-hazard risk analysis, which focuses on individual hazards in isolation, multi-hazard analysis considers how different hazards interact and depend on each other. This interaction can lead to complex and nonlinear relationships, making the analysis more intricate and demanding. Understanding the dependencies between hazards and their compound impacts is crucial for effective risk management and resilience planning (Hillier 2020). Turkey's Earthquake and flood in 2023 and the Tohoku earthquake followed by a tsunami in 2011 serve as compelling examples to illustrate the importance of considering interactions between hazards in multi-hazard-prone areas. For consistency and meaningful comparisons, it is important to assess the hazard level, vulnerability, and risk level of each hazard using an equivalent approach. This standardized methodology ensures the comparability of results and enables effective risk management strategies (Wang et al. 2020; Tyagunov et al. 2018; Kappes et al. 2012; Abdollahi and Vahedifard 2021).

In recent years, there has been an increasing focus on examining how cascading extreme events can interact with levees, potentially leading to their failure (Tyagunov et al. 2018). Quinn and Taylor (2014) promoted multi-hazard topography as a useful tool to demonstrate the advantages, effectiveness, and practicality of different levees. Selmi et al. (2022) presented a probabilistic approach to evaluating the liquefaction risk of an earthen flood protection levee by considering various groundwater tables over time. Zhang et al. (2023) conducted a probabilistic seismic assessment of earthen levees using advanced moment method formulations and the finite element method. Zimmaro et al. (2019) employed two distinct approaches to analyze the reliability of various segments within a levee system under earthquake and high-water level conditions. They utilized the Monte Carlo Method, known for its flexibility but computationally intensive nature, as well as the First Order Method (FORM), which is less computationally demanding but requires dividing the levee system into reaches with stationary limit state functions. Although they considered a multiple-hazard scenario, they did not extensively explore the interaction between flood events and seismic activity in their study.

Water Flow Through the Levees

In soils, interconnected voids enable fluids to move from high-energy zones to low-energy zones, making them permeable materials. It is crucial to measure and evaluate soil permeability accurately for estimating seepage in hydraulic structures and determining water quantities during dewatering operations (Elhakim 2016). Permeability is influenced by several factors, including the void ratio, the distribution of intergranular pores, and the degree of saturation. These factors collectively impact the ability of fluids to flow through the soil (Wang et al. 2021). Depending on the availability of data, permeability functions for soil can be obtained using empirical equations, analytical models, or statistical models (Leong and Rahardjo 1997). Based on how the parameters

change over time, steady-state and transient seepage analyses differ from one another. In steady-state analyses, the parameters stay the same, while in transient seepage analysis, the conditions at the hydraulic boundary, the amount of water in the area, and the ability of the soil to conduct water change over time (Tracy et al. 2016).

Levees function as a barrier protecting the adjacent lands from floods caused by seasonal/permanent rivers, and therefore, it is mostly unsaturated as the phreatic line passes through the middle of their bodies. It is the reason that unsaturated soil mechanics is of significance when dealing with the hydro-mechanical behavior of levees. Elevated water levels behind levees can lead to an increase in a hydraulic gradient within the structure, thereby raising the risk of under-seepage and through-seepage failures. Moreover, high water levels can exacerbate the impact of inadequate levee construction and weak foundation conditions, further enhancing the likelihood of failure during earthquakes (Rosidi 2007; Abdollahi and Vahedifard 2021; Giradi et al. 2023). The hydro-mechanical responses of unsaturated soils, such as water flow through the soil medium, volume change, and shear response are primarily influenced by matric suction which refers to the negative pressure within the pores of the soil and is mathematically defined below (Kim et al. 2018; Zhang and Lu 2019):

$$\psi_m = u_a - u_w \tag{2.1}$$

where denotes matric suction, stands for pore air pressure, and represents pore water pressure. The relationship between soil matric suction and volumetric water content, (defined as the volume of water in the soil divided by the total volume of the soil, (v_w/v), is defined as the soil-water characteristic curve (SWCC) which provides fundamental information to describe the mechanical

behaviors of soils (Fredlund and Xing 1994). Understanding this relationship is also essential when conducting transient seepage analysis (Van Genuchten 1980).

As shown in Figure 2.1, during the drying process, when the suction value is zero, the degree of saturation equals unity and the volumetric water content is equal to the porosity (n) and the volumetric of the soil. As the water begins to drain out of the soil, the matric suction increases from zero to the water content decreases a little and while the air begins to enter the soil through suction which is called Air Entry Value (AEV) or ψ_a. Then the soil starts to be desaturated more rapidly with increasing suction and this trend continues as the suction rises up to the value corresponding to the residual water content, θ_r at which the water phase becomes discontinuous and known as residual soil suction, ψ_r. During the wetting process, the steps mentioned above are reversed. As suction decreases, the soil gradually saturates, and the volumetric water content increases until reaching the full saturation. Over this process, where the water content begins to rise up too much is known as water-entry value, ψ_w (Yang et al. 2004).

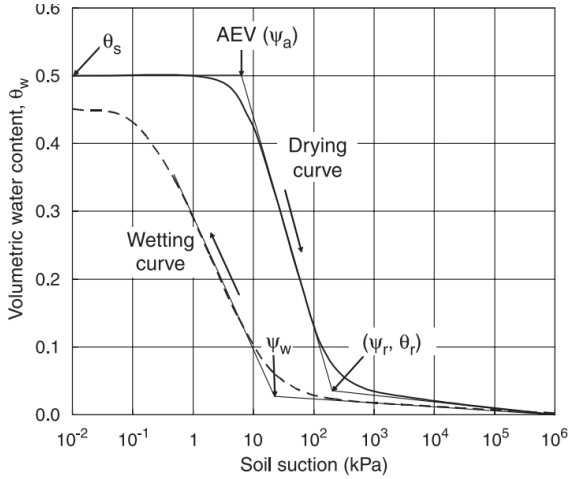

Figure 2.1 Soil water characteristic curves (SWCC)

After Yang et al. 2004

Based on the SWCC, a function that relates hydraulic conductivity to volumetric water content and matric suction is derived as a result of hydraulic conductivity. The soil permeability will be reduced due to fewer flow paths when the soil suction is high (lower saturation). As a result, in order to perform an accurate transient seepage analysis, one needs to estimate the SWCC accurately (Zhani et al. 2021).

To describe the SWCC numerous empirical models and equations were already provided by various researchers (e.g., Van Genuchten 1980; Mualem 1986; Fredlund and Xing 1994). The van Genuchten (1980) equation and the Fredlund and Xing (1994) equation were found by Leong and Rahardjo (1997) to be the best models to use for SWCC for a wide range of soil types.

To evaluate the SWCC of soils, Van Genuchten (1980) proposed below equation:

$$\theta_w = \theta_r + \frac{\theta_s - \theta_r}{\left[1 + \left[\frac{\psi_m}{a}\right]^n\right]^m} \tag{2.2}$$

where θ_w is the volumetric water content; θ_r is residual water content; θ_s is the saturated volumetric water content; a is a soil parameter related to the AEV of the soil; n is a soil parameter related to the rate of water extraction from the soil; and m is a soil parameter related to residual water content which is usually estimates using following equation:

$$m = 1 - \frac{1}{n} \tag{2.3}$$

Fredlund and Xing (1994) developed following equation for simulating of SWCC:

$$\theta_w = \theta_s \left[1 - \frac{ln(1 + \psi/\psi_r)}{ln(1 + 10^6/\psi_r)}\right]\left[\frac{1}{\{ln[e + (\psi/a)^n]\}^m}\right] \quad (2.4)$$

where ψ_r is the residual suction corresponding to the residual water content.

As a way of estimating SWCC, it can also be done by using the grain-size distribution of the soil (Perera at al. 2005). A number of prediction methods have been developed for this purpose, including those developed by Gupta and Larson (1979), Arya and Paris (1981), Haverkamp and Parlange (1986), Fredlund et al. (1997), and Aubertin et al. (2003). A study conducted by Yang et al. (2004) used these two equations to fit the SWCC test data of the drying and wetting five sandy soils and concluded that soils with a higher porosity tend to have a lower air-entry value as compared to soils with a lower porosity.

SEEP/W is a finite element software, which provided by GeoStudio package and it is capable of simulating the water flow though the soil media. It employs empirical predictors to simulate the performance of SWCC as a tool to estimate the variation in soil permeability with suction (Walshire and Robbins 2017). The following equation presents the governing differential equation for two-dimensional seepage in finite element method solve by SEEP/W throughout the soil medium:

$$\frac{\partial}{\partial x}\left(k_x(\theta)\frac{\partial H}{\partial x}\right) + \frac{\partial}{\partial y}\left(k_y(\theta)\frac{\partial H}{\partial y}\right) + Q = \frac{\partial \theta}{\partial t} \quad (2.5)$$

where H is total head; k_x and k_y is hydraulic conductivity in the x and y directions, respectively; Q is a boundary flux (usually equal to zero); θ is the volumetric water content, and t is the time (Likos and Lu 2004).

Slope Stability Analysis

Slope failure, commonly referred to as a slide, happens when a mass of soil beneath a slope moves downward and outward. This movement occurs primarily due to gravitational forces and seepage forces within the soil. Gravitational forces arise from the weight of the soil mass and the steepness of the slope, while seepage forces result from water movement in the soil. When these forces surpass the soil's strength, slope failure can occur (Zhang et al. 2011). Proper understanding and management of these factors are essential for evaluating and minimizing the risks associated with slope instability (Salunkhe et al. 2017). As a branch of geotechnical engineering, slope stability analysis can be viewed as a highly appropriate subject for probabilistic treatment, and it has attracted substantial attention in the literature as a result (Griffiths and Fenton 2004). Instability of natural slopes as well as man-made slopes, such as embankments for roads/railways, dams built hydraulically or by earth forces, is a major problem that needs to be addressed (Kaur and Sharma 2016).

There are a variety of methods such as limit analysis, strength reduction method and limit equilibrium by which the slope stability problems are analyzed. Among them, the limit equilibrium method is widely used for analyzing slope stability in both two and three dimensions (Azmoon et al. 2021). This approach is employed to identify potential failure mechanisms and calculate factors of safety for various geotechnical scenarios (Haung 2014). The commonly used limit equilibrium techniques for slope stability analysis also known as slices method include methods such as the ordinary method of slices (Fellenius), Bishop simplified method, Spencer method, and Morgenstern-Price method. The most developed slices techniques statically (or pseudo-statically) solves the problems by assuming a distribution of internal forces (Liu et al. 2015). In this technique, the sliding body is divided into smaller vertical slices, and the equilibrium conditions

of forces are considered for each slice to determine the tangential and normal stresses at the bottom of the sliding surface sections. This analysis helps assess the overall slope stability and the need for reinforcement measures (Kaur and Sharma 2016). This approach allows for the evaluation of slope stability based on the balance between shear strength and applied forces, providing a measure of safety against potential slope failure (Fredlund and Scoular 1999).

The Finite Element based strength reduction method is introduced as an alternative to the traditional limit equilibrium stability analysis. This method calculates the stability factor of a slope by considering the stress distribution in the soil obtained from a finite element analysis (Liu et al. 2015). In finite element analysis, slopes are divided into small elements, and a stress-strain relationship is determined for each element. This approach allows for a detailed analysis of the slope behavior by considering the interaction between the elements and their responses to applied forces or loading conditions (Duncan 1996).

The factor of safety is a numerical value that represents the margin of safety against failure in engineering and geotechnical analysis (Duncan 2000). When using the strength ruction method, the overall factor of safety for a slope can be defined as the available shear strength of the soil divided by the resisting shear strength. It represents the ratio between the strength of the soil and the forces acting on the slope, indicating its stability. The overall factor of safety combines the local factors of safety within the slope, and it modifies the fundamental assumptions inherent in the limit equilibrium definition of a factor of safety (Pesternack and Gao 1988).

In both limit equilibrium and finite element slope stability analyses, several key factors are essential for assessing the stability of a slope. These factors include the slope's geometry, the unit weight of the soil, the strength parameters (cohesion, c, and internal friction angle, φ) of the soil, and the forces acting on the slope (Khabbaz et al. 2012). In slope stability analysis, the resisting

force for each slice is estimated based of the shear strength parameters at the center of the slice, multiplied by the base area of the slice (Fredlund and Scoular 1999). Understanding and considering these factors are vital for accurately evaluating and predicting the stability of a slope using either limit equilibrium or finite element methods.

Soil shear strength is a crucial parameter for predicting slope and embankment stability, foundation-bearing capacity, and pressures on earth-retaining structures. The Mohr-Coulomb theory is widely used to simulate the shear strength of saturated soils (Das 2010). The shear strength of unsaturated soil is influenced by the soil water content and, consequently, by matric suction (Vanapalli et al. 1996; Khalili and Khabbaz 1998). In unsaturated soils, positive pore water pressure decreases shear strength by reducing effective stress, while negative pore water pressure increases strength by increasing effective stress (Olson 1963). To determine the shear strength of unsaturated soils two approaches are proposed by Fredlund et al. (1978) and Bishop (1959). Bishop (1959) estimated the shear strength base on the effective strength factors $C', \emptyset'$ and define as below:

$$\sigma' = (\sigma - u_a) + \chi(u_a - u_w) \tag{2.6}$$

where σ is the total stress, u_a is the pore air pressure, u_w is the pore water pressure, c' the effective cohesion, $\emptyset'$ is the effective angle of internal friction σ' is the total stress and χ is the effective stress parameter and it is equal to 1 for saturated soils and 0 for dry soils.

Shear strength is then determined through Mohr-Coulomb failure criteria. Khalili and Khabbaz (1998) expressed the below equation as the best fit between χ and the suction ratio:

$$\chi = [\frac{(u_a - u_w)}{(u_a - u_w)_b}]^{-0.55} \quad (2.7)$$

where $(u_a - u_w)_b$ is the air entry value determined from the SWCC.

On the other hand, Fredlund et al. (1978) introduced a linear shear strength equation with matric suction as listed below:

$$\tau = c' + (\sigma - u_a)tan\emptyset' + (u_a - u_w)tan\emptyset^b \quad (2.8)$$

where $\emptyset^b$ is the angle of internal friction with respect to matric suction $(u_a - u_w)$.

This approach is not widely implemented in practice due to the high costs and time involved in laboratory testing, the expensive and complex equipment required, and the specialized expertise needed. Therefore, they proposed two different empirical equations estimating $tan\emptyset^b$(Vanapalli et al. 1996), as expressed in next equations:

$$tan\emptyset^b = \left(\frac{\theta}{\theta_s}\right) tan\emptyset' \quad (2.9)$$

$$tan\emptyset^b = \left(\frac{\theta - \theta_r}{\theta_s - \theta_r}\right) tan\emptyset' \quad (2.10)$$

where θ is volumetric water content; θ_s is saturated water content and θ_r is residual volumetric water content.

Dynamic Response of Levees

As a secondary effect of earthquakes, liquefaction phenomena are considered to be less hazardous than those associated with landslides and tsunamis triggered by seismic activity

(Perucca and Moreiras 2006). Liquefaction potential is the likelihood of soil losing its strength and stiffness during seismic activity. It is evaluated by comparing earthquake loading and liquefaction resistance using measures such as cyclic shear stress amplitude. Seed and Idriss (1971) were among the first researchers assessed the liquefaction potential of soils and it is frequently evaluated using simplified procedures originally proposed by them, using a standard penetration test (SPT). If the factor of safety, which is the ratio of cyclic resistance to cyclic stress, is less than or equal to one, then liquefaction of soil is expected to occur. Similarly, a factor of safety greater than one predicts no soil liquefaction. In order to evaluate liquefaction, Seed and Idriss (1971) proposed the cyclic stress ratio (CSR) as follows:

$$CSR = 0.65 \cdot \left(\frac{\sigma_v}{\sigma'_v}\right) \cdot \frac{a_{max}}{g} \cdot r_d \tag{2.11}$$

where 0.65 is a coefficient used to calculate the equivalent uniform stress cycles for an earthquake, ensuring the generation of the same pore water pressure; σ'_v is the effective vertical stress; a_{max} is the maximum acceleration amplitude of the earthquake ground motion; g is the acceleration due to gravity (9.81 m/s^2); and r_d is the depth-related stress reduction factor that varies with depth (z) from the ground surface.

Soil liquefaction resistance is expressed as cyclic resistance ratio (CRR), which can be calculated using several in-situ tests (Yegian and Whitman 1978). These tests including standard penetration test (SPT), cone penetration test (CPT), and shear wave velocity (V_s) tests. The FoS for an earthquake of magnitude, M_w, is:

$$FoS = \frac{(CRR)_{Mw=7.5}}{CSR} \cdot MSF \tag{2.12}$$

The magnitude scaling factor MSF accounts for ground motion duration effects and adjusts the equivalent uniform shear stress produced by a magnitude M_w earthquake into its equivalent CSR for an earthquake with the magnitude of M_w=7.5. Many expressions have been proposed in the literature for evaluating MSF. For 7.5-magnitude earthquakes, MSF can be expressed as below equations:

$$MSF_{min} = \frac{10^{2.24}}{M_w^{2.56}} \tag{2.13}$$

$$MSF_{max} = (\frac{M_w}{7.5})^{-3.3} \tag{2.14}$$

To take a conservative approach, we will use only one limit (MSF_{min}) and label it as MSF. CSR and CRR change with depth, so the liquefaction potential is evaluated at different depths within the soil profile. Soil with FoS less than one is generally considered liquefiable, while soil with FoS more than one is classified as non-liquefiable.

Relying solely on the SPT for geotechnical analysis may not always be feasible in every location. To address this limitation, QUAKE/W, a geotechnical software available commercially in the GeoStudio package, is utilized for dynamic analysis of earth structures subjected to earthquake shaking and other seismic loadings. QUAKE/W offers a comprehensive toolset for assessing the response of geotechnical systems under dynamic loading conditions, providing valuable insights into the behavior of earth structures during seismic events.

When a saturated sandy layer is overlaid by a particular thickness of confining material, such as clay or silt, rapid drainage is impeded, creating conditions conducive to liquefaction

(Obermeier et al. 2005). Analysis of recent earthquakes has shown that liquefaction can occur in sandy-layer soils, leading to phenomena such as sand boiling, ground cracking, and lateral spreading. Notably, liquefaction has been observed even in areas with moderate seismic intensity and at considerable depths (Huang and Yu 2013). The findings highlight the potential hazards and complexity of liquefaction in sandy layer soils during seismic events. The potential for soil to liquefy is influenced by many variables in addition to grain sizes (Haldar and Tang 1979). When the grain structure collapses, the sand can fail and shear at strengths well below the strength represented by conventional effective strength parameters c' and $\emptyset'$. That is, the sand can become mobile at a c' and $\emptyset'$ much lower than the conventional effective c' and $\emptyset'$. If we have the stress state and path in the q-p' (deviator stress versus mean normal stress) space, we have a critical state line that represents point failure. Two of the more important variables that influence the potential for soil liquefaction are the void ratio and the stress state. Deviator stress (q) is the shear in soil and means effective stress (p') is the confining stress and they can be calculated using the following equations:

$$q = \sigma_1 - \sigma_3 \tag{1.15}$$

$$p' = \frac{\sigma_1' + \sigma_2' + \sigma'_3}{3} \tag{1.16}$$

Critical state line (CSL) represents strength at large strains when shear resistance and the volume remain constant with ongoing strain. It refers to the steady-state strength and also it sometimes refers to residual strength and the slope of CSL can be calculated using the below equation.

$$M = \frac{6sin\emptyset'}{3 - sin\emptyset'} \tag{2.17}$$

In the diagram shown in Figure 2.2, when a sample is isotopically consolidated at point A, the effective stress path during undrained monotonic loading follows the curve illustrated. Initially, the shear stress increases, but then it curves back to the left and reaches a maximum, causing the soil-grain structure to collapse. This collapse results in a sudden rise in pore pressure and a rapid decrease in strength until it reaches a steady-state strength. In other words, liquefaction is initiated at the point of collapse in this scenario (GeoStudio 2022).

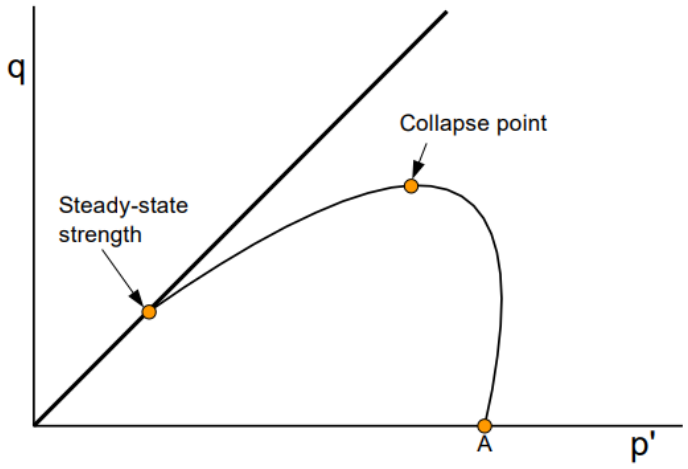

Figure 2.2 Undrained monotonic shear of loose sand under undrained loading GeoStudio 2022

In Figure 2.3, a set of experiments was conducted on triaxial specimens that had identical initial void ratios but were consolidated under different confining pressures. By plotting the data, it is possible to draw a straight line that passes through the point representing the steady-state strength and continues through the peaks or collapse points observed in the tests. Sladen et al.

(1985) termed this line a Collapse Surface. Hanzawa et al. (1979) and Vaid and Chern (1983) contradicted the initial hypothesis, proposing that the line passing through the collapse points intersects the plot origin (zero shear stress, zero mean stress), not the steady-state strength point. They referred to this line as a "Flow Liquefaction Surface." QUAKE/W offers the capability to utilize the steady-state strength and the collapse surface to identify elements that may be susceptible to liquefaction (GeoStudio 2022).

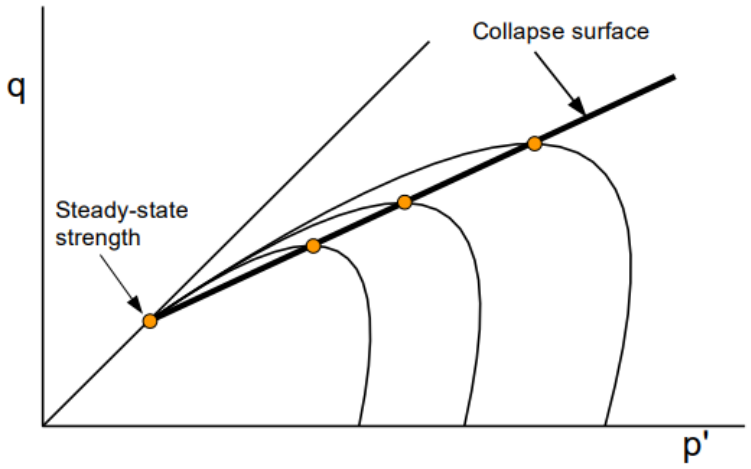

Figure 2.3 Surface collapse

GeoStudio 2022

There is a possibility that cyclic loading could lead to liquefaction, as illustrated in Figure 2.4. If we take a sample of soil that was initially at stress state point B, when that soil is subjected to cyclic loading, the pore pressures within the soil will gradually rise until the stress cyclic path intersects the collapse surface. At this point, the soil undergoes liquefaction, resulting in a sudden decrease in strength along the collapse surface, ultimately reaching the steady state point. The occurrence of this phenomenon highlights the vulnerability of soils to liquefaction, especially

under situations of cyclic loading, which can have major implications for engineering and geotechnical applications (GeoStudio 2022).

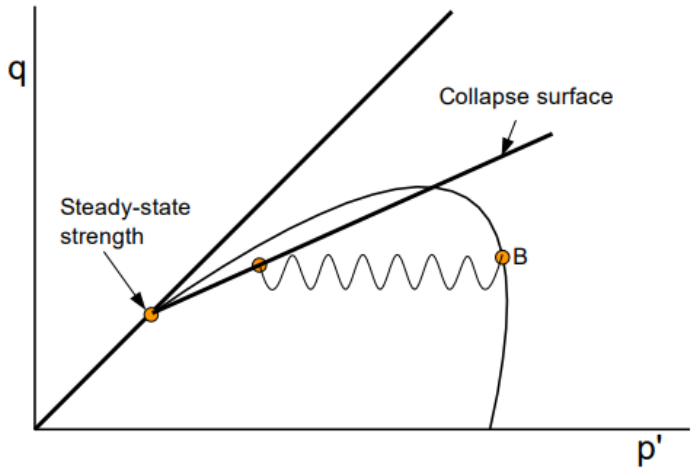

Figure 2.4 Undrained cyclic loadings leading to the liquefaction incident GeoStudio 2020

Land sliding triggered by strong shaking is a significant contributor to earthquake damage. The ability to predict earthquake-induced landslide movement is an important aspect of seismic hazard analysis and the design of slopes that are earthquake resistant. Newmark's sliding block analysis, developed by Newmark (1991), offers a practical method for predicting earthquake-induced landslide displacements. It models a landslide as a rigid-plastic block moving along an inclined plane. This approach provides a more useful estimation of landslide displacements compared to pseudo-static analysis, which makes simplifying assumptions. By considering the dynamic behavior of the landslide mass, Newmark's sliding block analysis allows for more accurate predictions of approximate landslide displacements (Jibson 1993).

The Newmark method aims to identify the moments during seismic shaking when a slope loses stability, i.e., when the factor of safety drops below one. It focuses on capturing the time

intervals when the slope experiences movement and the ultimate goal is to accumulate these movements. T determine the settlement of the geo-structure using the Newmark method, the acceleration of each element is required in addition to the factor of safety. Hence, while the acceleration is known at every single moment of instability condition, the integration of acceleration over time at which the safety factor is less than unity would be velocity and the integration of calculated velocity on time could provide displacement of the structure. However, this method is applicable in specific situations. It is most suitable for cases where the primary concern is inertial forces and where there is minimal loss of shear strength due to excess pore pressure generation (Jibson 1993; Yang 2021).

Probability of coincidence of two events

The annual probability of one or more coincident exceedance events refers to the likelihood of multiple events occurring simultaneously or overlapping within a given time frame, typically a year. This concept is often used in the field of risk assessment, particularly when analyzing the occurrence of multiple rare events or hazards. Elingwood (1995) conducted research on the event coincidence analysis for the design of the U.S. Army Corps of Engineers navigation structures. In this method, the annual probability of an earthquake coincident with a flood is defined as below:

$$p = \lambda_{12} = \lambda_1 \, \lambda_2 \, (\tau_1 + \tau_2) \tag{2.18}$$

where λ_1 is the annual exceedance probability of earthquake; λ_2 is the annual exceedance probability of flood; τ_1 is the mean duration of earthquake (year) and τ_2 is the mean duration of flood (year). Since the duration of the earthquake (τ_2) is typically measured in seconds, τ_2 (yr) << τ_1 and it is assumed to be negligible (i.e., zero).

CHAPTER III

NUMERICAL MODELING

Introduction

Despite earthquakes occurring less frequently than floods, levees are more susceptible to damage by earthquakes. Since 1850, California and its surrounding regions have been subjected to 167 earthquakes of magnitude 6 or higher. These data indicate that approximately 1.1 such events occur each year. Additionally, since 1812, there have been earthquakes roughly every five years with magnitudes between M 6.8 and 6.5 (Toppozada and Branum 2004).

Over decades ago, extensive research has been conducted to understand how liquefaction occurs and the mechanisms involved in it to improve our understanding. These studies have improved our understanding of soil dynamics, and that knowledge has enabled us to develop effective techniques for predicting and mitigating liquefaction hazards (e.g., Seed and Idriss 1971; Poulos et al. 1985; Ishihara 1993; Toprak and Holzer 2003; Jefferies and Been 2015; Selmi et al. 2022).

Although previous studies have brought so much progress, it is worth noting that the annual probability of co-occurring floods and earthquake events has been considered rarely, if any. In this study, a novel approach has been provided to assess the vulnerability of levees to simultaneous floods and earthquakes. To this purpose, we used the GeoStudio available finite element software package, which includes SLOPE/W, SEEP/W, SIGMA/W, and QUAKE/W modules to model the Elkhorn levee in Sacramento County, California under the compound influence of floods and

seismic loading. The Fault Tree Method is further used to determine the reliability of the levee by considering the probability of coincidental floods and earthquakes occurring subsequently. As a result, this contributes to the development of updated risk assessments for geo-structures in areas of high risk.

Case Study

Because of the high population density, a concentration of levees, and a multitude of possible reasons for levee failure, such as earthquakes, heavy rains, and poor maintenance, the Sacramento-San Joaquin Delta region is an extremely high-risk area to natural disasters. About 738,00 acres of land are part of the Sacramento-San Joaquin Delta, and they are mostly rural in nature. They are protected by a network of 1,800 kilometers of levees that runs the entire length of the Delta. (Flynn 2007; Abdollahi and Vahedifard 2021). The Elkhorn Levee has been described as one of the most prominent levees in Sacramento County, California, and has been studied previously by Khalilzad et al. (2014), Vahedifard et al. (2020), and Abdollahi and Vahedifard (2021). Figure 3.1 illustrates a typical cross-section of the Elkhorn Levee.

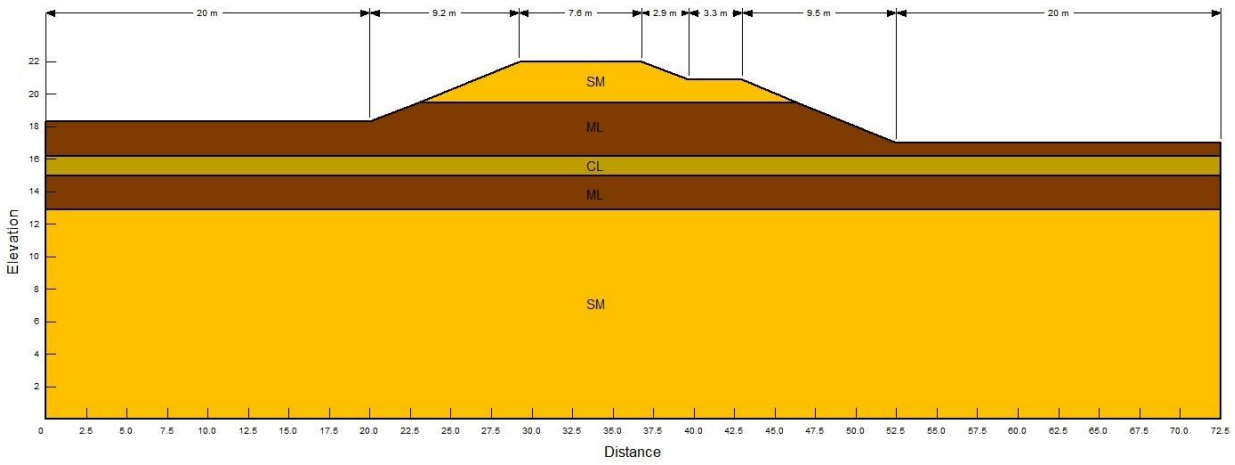

Figure 3.1 Elkhorn levee cross section

Aafter Vahedifard et al. 2020

Table 3.1 indicates the soil properties of each layer of the levee including silty sand (SM) of the embankment and foundation layers, silty layer (ML), and clayey layer (CL) which are provided by Abdollahi and Vahedifard (2021).

Table 3.1 Soil properties of Elkhorn levee

Parameter	$\gamma\ (\frac{K}{m^3})$	$E\ (kPa)$	$c'(kPa)$	$\emptyset'(°)$	PI
SM Embankment	18.0	1.47×10^4	1	34	5
ML	18.0	3.48×10^3	5	30	10
CL	18.4	8.62×10^4	5	28	20
SM Foundation	17.0	1.47×10^4	1	32	5
$\boldsymbol{\gamma}$: unit weight; $\boldsymbol{E}$: elasticity modulus; $\boldsymbol{c}'$: cohesion; $\boldsymbol{\phi}'$: friction angle; PI: plasticity index					

Comparison Elkhorn levee soil layers properties include unit weight, elasticity modulus, cohesion, friction angle, plasticity index (Abdollahi and Vahedifard 2021).

Analysis of the Seepage

To evaluate the impact of different floods intensity and duration on the levee of interest, SEEP/W software was used to model both steady-state and transient flow conditions. Different

flood duration is applied to the levee based on the elevation of the water level behind the upstream side. In other words, the elevation of the water level is regulated so that the normal water level is reached at the end of the flood time duration. Additionally, several models were developed to simulate the rapid drawdown phenomenon afterward the phreatic line reaches its steady state.

Streamflow and flood level data provided by Vahedifard et al. (2020) were used to assess the water levels corresponding to the design streamflow for various recurrence intervals. This information was provided in Table 3.2, which made it possible for us to analyze and compare different streamflow scenarios and therefore provide us with valuable insight into the design of resilient infrastructures based on these data.

Table 3.2 Floods water level

Recurrence interval (years)						
Years	10		25		50	
Flood loading	Historical	Future	Historical	Future	Historical	Future
Flood Level (m)	18.33	20.46	19.54	21.38	20.56	21.9

It shows level of water for different historical and future flood return periods for Elkhorn levee (after Vahedifard et al. 2020).

Based on the position of the soil layers relative to the water level, we categorized their analysis type when running SEEP/W. Layers below the water level were considered saturated, while layers above the water level were considered unsaturated. Using this distinction, water flow and pore pressure conditions within the soil profile could be appropriately modeled.

As mentioned before when the suction value is zero, the degree of saturation, S_r equals unity and the saturated volumetric water content (θ_s) is equal to the soil porosity (n). Therefore, by having the value of void ratio, e, from Table 3.1, we estimated the value of volumetric water content for each layer which is required when running a saturated/unsaturated analysis via Seep/W.

In this study, the soil water retention curves provided in the GeoStudio library were used to establish the correlation between matric suction and soil water content in unsaturated layers. For the steady-state analysis, a total head of 18.3 m was applied as the boundary condition on the upstream side of the levee, while a total head of 17 m was assigned to the downstream side of the levee under investigation. In order to determine the hydraulic conductivity of unsaturated layers, we used Fredlund et al. (1994) model. To this purpose, as mentioned before, residual water content, θ_r determined using SWCC at which the water phase becomes discontinuous. Also, permeability in vertical and horizontal directions of each layer used as provided by Abdollahi and Vahedifard (2021) and presented in Table 3.3.

Table 3.3 Soils water content and hydraulic conductivity

Parameter	e	θ_s	θ_r	$K_{sat}(\frac{m}{s})$	k_y/k_x
SM Embankment	0.36	0.26	0.02	6.37×10^{-5}	1.00
ML	0.50	0.33	0.05	6.37×10^{-7}	0.50
CL	0.52	0.35	-	6.37×10^{-9}	0.25
SM Foundation	0.45	0.31	-	6.37×10^{-7}	1.00
e: void ratio; θ_s: saturated water content; θ_r: residual water content; $\boldsymbol{k_{sat}}$: saturated hydraulic conductivity; $\boldsymbol{k_y}$ ***and*** $\boldsymbol{k_x}$: hydraulic conductivity in vertical and horizontal directions					

It shows soil parameters including void ratio, saturated water content, residual water content, saturated hydraulic conductivity and hydraulic conductivity ratio of different soil layers of Elkhorn levee (Abdollahi and Vahedifard 2021; Budhu 2010)

For the purpose of conducting the transit seepage analysis, the water level behind the levee was gradually increased at a constant rate of 5 cm per hour until the peak flood level was reached for each flood scenario by the gradual increase of water level behind the levee.

Following the flood peak level, it was maintained for several days until a steady-state condition was achieved. Throughout these two stages, the downstream slope was treated as a

potential seepage surface, allowing water flow, while the bottom boundary remained impermeable, preventing any water movement through it.

Initial Stress State

Stress distribution within the soil medium is a key factor via which the susceptibility of structure to excessive deformation as well as possible failure is determined. In this study, SIGMA/W software is employed to find the initial stress-strain state at each point of the geo-structure of concern. To this purpose, Mohr-Coulomb elastic plastic constitutive model is utilized and the relevant parameters are chosen based on experimental results reported by Abdollahi and Vahedifard (2021) and shown in Table 1. The permanent settlement and stresses due to the body loads are then determined and used as the initial condition of the dynamic analysis.

The pore water pressure and resulting effective stress are calculated through the drained analysis method. The imposed loads include body forces along with the hydro-static pressure of the water. Seepage forces are considered via compound FE formulation used by the concurrent run of SIGMA/W and SEEP/W software. Deformation contours as well as stress invariants are determined as the direct outcomes of the analysis carried out under monotonic loadings.

Analysis of the Seismic Response

Sacramento has relatively low levels of natural hazards as compared with other cities in the state. There are a number of factors that contribute to this favorable status, including the low seismic activity history of the region. Due to this, the probability of a ground motion causing various levels of discomfort in Sacramento is generally lower than that of other areas in the country (Burton and Cutter 2008). However, it is crucial to recognize that no region in California can

completely dismiss the possibility of future earthquakes. Despite experiencing lower hazard levels, Sacramento is still at risk of experiencing significant ground motions.

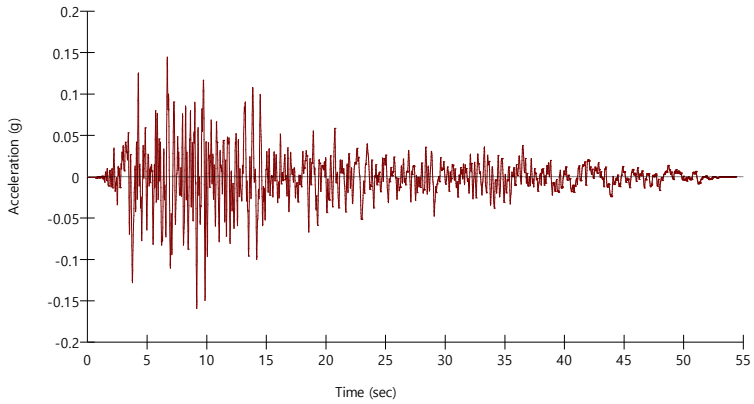

Figure 3.2 Time history acceleration

ngawest2.berkeley.edu

In this study, we used the 1952 Kern County earthquake time history which occurred on July 21, 1952 with magnitude of 7.3 and peak ground acceleration (PGA) of near to 0.16g in the southern San Joaquin Valley, and we applied it as the seismic loading at the base of the levee's foundation. Figure 3.2 illustrates the time history of the horizontal ground acceleration of the earthquake. We analyzed various earthquake scenarios for the Sacramento region by considering four different earthquakes return periods. To this purpose, the maximum peak ground acceleration values for each scenario were obtained from several maps provided by USGS (2022). These maps, shows the maximum peak ground acceleration in different regions of the United States for different return periods. Figure 3.2, shows the PGA variation for 144-year earthquake return period. We modified the time history data of the 1952 Kern County earthquake by adjusting it to match the new peak ground acceleration values obtained from Chowdhury's research. This allowed us to study the potential effects of different earthquake intensities on the Sacramento region. Table 3.4,

illustrates the maximum peak ground acceleration for different return period that we adopted from the hazard map provided by USGS (2022).

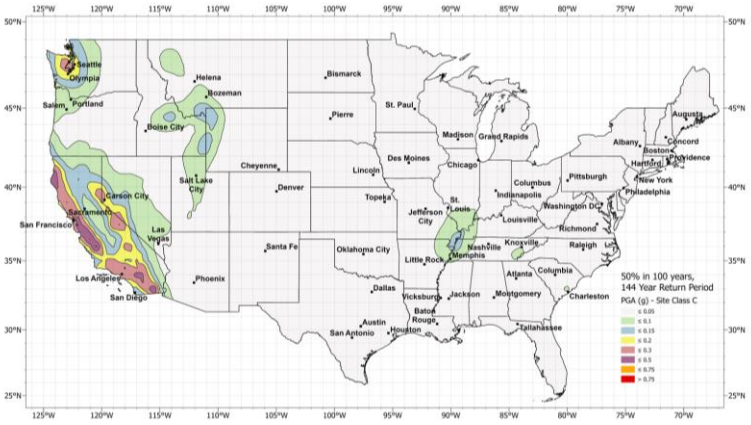

Figure 3.3 144-year earthquake return period hazard map

USGS 2022; Chowdhury 2023

Table 3.4 Maximum ground peak acceleration

EQ Return period (year)	144	475	975	2475
Maximum PGA (g)	0.15	0.2	0.3	0.5

This illustrates the maximum probable ground peak acceleration for different earthquake return periods for Sacramento, California region (USGS 2022)

Seismic Analysis Parameters

Poisson's ratio is a dimensionless value that related to the deformation behavior of a material when subjected to stress. It describes the relationship between lateral and longitudinal strain in a soil material under uniaxial loading (e.g., Salem 2000; Fredlund et al. 2012; Kumar Thota et al. 2021). Poisson's ratio for soils can range from 0 to 0.5, depending on factors like soil type, density, confining pressure, porosity, and degree of saturation (e.g., Salem 2000; Velea et al. 2000; Inci et al. 2003; Gao et al. 2013; Suwal and Kuwano 2013; Kumar Thota et al. 2021). The Poisson's ratio is nearly zero when a stiff soil specimen is loaded uniaxially and there is no lateral

movement. When the soil specimen's volume does not change, Poisson's ratio reaches 0.5. Clays generally have a Poisson's ratio between 0.20 and 0.45. Silts typically have a Poisson's ratio between 0.20 and 0.35, while that of sands ranges from 0.15 to 0.35 (Budhu 2010; Fredlund et al. 2012; Kumar Thota et al. 2021).

Studies have shown that the Poisson's ratio tends to increase with the increase in soil saturation. Despite this, Poisson's ratio models, as well as models based on their effects on Poisson's ratio, are rare to be identified in the literature as a means of explicitly capturing the effect of saturation (Oh and Vanapalli 2018; Kumar Thota et al. 2021). Table 3.5 illustrates, a database of experimental data of the Poisson's ratio and the relevant references for different soil layer of the levee which are used when analyzing the models via Quake/W and adopted by Kumar Thota et al. (2021).

Table 3.5 Poisson's ratio for different soil layers

Soil type	ν	Reference
SM (Silty sand)	0.47	Byun et al. (2013)
ML (Bonny silt)	0.43	Kumar Thota et al. (2021)
CL (Lean Clay)	0.41	Inci et al. (2003)

It shows Poisson's ratio for different Elkhorn levee soil layers and it references for each one (Kumar Thota 2021).

Another important parameter in the dynamic analysis is Young's modulus (E). In the elastic response of soil, it is the constant of linear proportionality in which stress is incrementally proportional to strain, and it can be calculated from the equation below:

$$\delta\sigma = E\ \delta\varepsilon \tag{3.1}$$

where $\delta\sigma$ is the increment of total stress, E is the module of elasticity, and $\delta\varepsilon$ is the strain increment.

In QUAKE/W software all stiffness properties are specified with the shear modulus G which is determined as below:

$$G = \frac{E}{2(1+\nu)} \tag{3.2}$$

In this study, we used equivalent linear model in QUAKE/W which modify the stiffness of the soil in response to computed strain. QUAKE/W analyzes each Gauss numerical integration point in the earthquake record to identify peak shear strains. When soil experiences dynamic stresses, it tends to soften due to cyclic shear strain. This ratio is referred to as a G-reduction function in the Equivalent Linear model. The cyclic shear strain is obtained from the finite element analysis. By considering the computed shear strain, the G-reduction function, and the specified G_{max}, new G values are calculated for each iteration of the analysis. This process is repeated until the shear modulus has been modified according to a specified G reduction function. This procedure continues until the required G modifications are within a specified range (GeoStudio 2022).

When confining or overburden stress increases, soil stiffness generally increases. In QUAKE/W, $G_{\max}$ values can be specified as functions to capture this behavior. $G_{\max}$ of cohesive soils can be estimated by Hardin and Drnevich (1972), Hardin (1978), and Mayne and Rix (1993) based on the following equation:

$$G_{max} = 625 \left(\frac{1}{(0.3+0.7e^2)}\right)(OCR)^k\sqrt{P_a\sigma'_m} \tag{3.3}$$

where e is the void ratio; OCR is the over-consolidation ratio; P_a is atmospheric pressure; σ'_m is the mean effective stress.

Also, k is an exponent related to the soil plasticity index (PI) and is estimated using equation below.

$$k = \frac{PI^{0.72}}{50} \tag{3.4}$$

In QUAKE/W it is possible to estimate the G_{max} function using the parameters including OCR, e, PI and k_0 (at-rest earth pressure coefficient). The value of OCR we used in our modeling is equal to one for all saturated layers. k_0 is determined based on the elasticity as follows:

$$k_0 = \frac{\nu}{1-\nu} \tag{3.5}$$

The QUAKE/W software uses several equations developed by Ishibashi and Zhand (1993) to estimate the ratio of shear modulus to maximum shear modulus (G/G_{max}) as a function of shear strain. It also considers the connections between G/G_{max}, plasticity index (PI), and confining pressure provided by Kramer (1996). By doing so, the software creates a function that is specifically designed for a given PI and a specified confining stress.

Similar to G_{max}, the damping ratio (ξ), in QUAKE/W can be defined either as a constant value or as a function. Ishibashi and Zhang (1993) developed an equation, discussed by Kramer (1996), to estimate the damping ratio function. It considers variables such as plasticity index (PI), G modulus reduction ratio (G/G_{max}), and indirectly, the confining pressure and presented as below:

$$\xi = 0.333\,\frac{1+\exp\left(-0.0145PI^{1.3}\right)}{2}\left[0.586\left(\frac{G}{G_{max}}\right)^2 - 1.547\frac{G}{G_{max}} + 1\right] \tag{3.6}$$

The formula for the damping ratio mentioned earlier was originally formulated with confining pressures expressed in units of *kPa*. However, it is essential to emphasize that the damping ratio is not significantly affected by the specific units used for confining pressure. It should be noted that the expression for G/G_{max} was specifically derived for pressures in *kPa* units.

During earthquake shaking, pore-pressures are determined by the number of uniform cycles, *N*, for the earthquake and the number of cycles, N_L, that will cause liquefaction in a particular soil. To find the pore pressure ratio (r_u), QUAKE/W uses equation below provided by Lee and Albaisa (1974) and DeAlba et al. (1975):

$$r_u = 0.5 + \frac{1}{\pi}\, sin^{-1}\left[2(\frac{N}{N_L})^{1/\alpha} - 1\right] \tag{3.7}$$

QUAKE/W uses this equation to estimate a pore pressure function which is possible to estimate various functions by entering the value of α which is originally is the fitting parameter of SWCC proposed by Fredlund and Xing (1994). In this study, we used the value of 0.7 for α recommended by GeoStudio (2022) to estimate pore water pressure function.

The Cyclic Stress Ratio (CSR) in soil analysis is related to the number of cycles needed for liquefaction. This relationship is described by the Cyclic Number function. It helps assess soil susceptibility to liquefaction under dynamic loading conditions. Seed and Lee (1965), conducted cyclic testing on Sacramento River Sand. They categorized the sand into Loose, Medium Loose, Medium Dense, and Dense samples and proposed the relevant equations accordingly. QUAKE/W provides the user with the choice of each soil type and eventually, the cyclic number. In this study, the appropriate compaction condition is assigned to each soil layer based on the void ratio (dry unit weight) of each soil type.

To assess the levee displacement, QUAKE/W uses the Newmark deformation analysis method, provided by Newmark (1965). A slope's actual acceleration is calculated by this method when the static yield acceleration is greater than the slope's actual acceleration. Using the Newmark method, slope slides can be analyzed using the seismic acceleration history. By identifying critical points during seismic shaking, stability can be compromised. When the factor of safety falls below one, there will be some movement on the slope. To perform Newmark analysis, it is necessary to couple the QUAKE/W module and the SLOPE/W module of the Geo-Studio program. This coupling is essential in order to obtain the dynamic stress of the slope. By integrating these modules, the dynamic stress can be calculated effectively for the analysis. By determining the specific value of the initial in situ stress, we can get the static stress, and by using the QUAKE/W program, we can get the vibration stress. In order to calculate the dynamic stress, we subtract the initial static stress from the vibration stress. This calculation is based on the following formula:

$$\sigma_{Dynamic} = \sigma_{Quake} - \sigma_{Static} \tag{3.8}$$

where σ_{Quake} is the static plus dynamic stress in the ground, and σ_{Static} is initial insitu stress state conditions.

SLOPE/W calculates the displacements for every trial slide surface, allowing us to identify those with the highest displacement. To identify the slide with the maximum displacement, the surfaces of trial slides can be classified based on their deformation instead of relying solely on the safety factor. The approach provides a convenient method for assessing and confirming which slide exhibits the largest displacement.

Slope Stability Analysis

Modeling the Elkhorn levee using SLOPE/W software enables us to assess its stability against instability in both static and pseudo-dynamic states. This powerful geotechnical tool allows us to analyze factors of safety and potential failure modes under various scenarios, encompassing compound relevant earthquakes and floods, steady-state conditions, and rapid drawdown events. To begin the analysis, the SLOPE/W software utilizes geotechnical data, such as soil properties, groundwater conditions, and levee geometry. A static analysis is conducted to determine the factor of safety against slope failure during typical conditions. The software considers the static loads from the levee's self-weight and hydrostatic pressures from steady-state flooding.

Next, pseudo-dynamic analyses are performed to assess the levee's stability under seismic events compound with flood conditions. These pseudo-dynamic scenarios provide critical insights into potential failure mechanisms during seismic events.

Additionally, the software examines rapid drawdown conditions, where water levels decrease rapidly due to the end of flood events or levee damage. This analysis helps identify potential issues with quick changes in water pressures and their impact on the levee's stability.

Fault Tree Probabilistic Analysis

The Fault Tree Method is a systematic approach used in probability analysis to evaluate the failure probability of complex systems. It involves representing the potential failure modes of the system in a graphical manner, with the top event (system failure) at the root node and the contributing basic events and intermediate events below. The logic gates (AND, OR) are used to define how these events compound to cause the top event. By quantifying the probabilities of basic events and considering logical relationships, the Fault Tree Method allows analysts to calculate the overall probability of system failure and identify critical events that contribute most

significantly to the system's unreliability. This method is widely applied in various industries, including engineering, safety assessment, and risk analysis.

This method is employed in the current study to determine the probability of the studied levee under compound flood and earthquake. To this purpose, the AND operator is used when the co-occurrence of flood and earthquake is considered. Different scenarios of floods/quakes are getting together via the OR operator. Also, different failure mechanisms are related to the OR operator. The occurrence of failure under compound loading is associated with each flood/earthquake scenario through the AND operator (Lee et al. 1985).

Conclusion

In this chapter, we detailed our utilization of four robust modules within the GeoStudio software to assess the hydro-dynamic response of the Elkhorn levee under the compound loadings of flooding and earthquakes. To examine the flux, hydraulic gradient contours, and pore pressure distribution, we employed SEEP/W

To understand how floods and earthquakes could impact the levee in different situations, we looked at two different situations where floods and earthquakes could happen together. In the first scenario, we assumed that an earthquake might occur during the peak of a flood, when the water level is at its highest. To study this, we kept the water level at the peak for several days until a steady-state condition reaches. In the second scenario, we considered the possibility of an earthquake happening after the flood, when the water level returns to its initial state. For this case, we simulated a rapid drawdown scenario after the peak water level reached the steady-state condition.

The evaluation of initial stress-strain states was performed using SIGMA/W. Additionally, we explained on the slope stability analyses, carried out by SLOPE/W, considering both static and pseudo-dynamic conditions.

Furthermore, we provided a comprehensive explanation of how the Newmark method was applied to calculate quake-induced permanent deformation, and how QUAKE/W aided in identifying liquefiable zones. To address failure probability, we employed the Fault Tree Method, which we also described in detail.

CHAPTER IV

RESULT AND DISCUSSION

Introduction

In this chapter, we present the outcomes of our comprehensive numerical analysis, employing four powerful modules of the Geo/slope software package including Seep/W, Sigma/W, Slope/W, and Quake/W, to evaluate the performance of the levee named "Elkhorn" under compound flood and earthquake loadings. Through an array of scenarios involving varying flood and seismic conditions, we examine the levee's response to these dynamic forces and assess critical geotechnical parameters.

The evaluation begins with a focus on flux and hydraulic gradients, as we investigate the flow of porewater and analyze water pressures under different load compound. This investigation will allow us to understand how the levee's foundation and internal stability are affected by the interaction of floodwater and earthquake-induced vibrations.

Next, we delve into porewater pressure, maximum mean effective stress, and maximum deviator stress to gain insights into the levee's stability under the compound loadings. These findings will help us identify potential failure mechanisms and areas of concern, thus aiding in the design and management of the levee for enhanced resilience. As we progress, we scrutinize the factor of safety along with Newmark deformations and liquefaction potential. These crucial analyses will provide a comprehensive understanding of the levee's stability against seismic loads

and highlight the potential for liquefaction-induced ground failures, a critical consideration for the safety of the surrounding infrastructure and communities.

Through this chapter, we aim to present a thorough exploration of the numerical analysis results, shedding light on the levee's performance under various flood and seismic scenarios. Our findings will not only contribute to a deeper understanding of the Elkhorn levee's behavior but also serve as valuable insights for the design and assessment of levee systems facing similar multi-hazard challenges.

Seepage Analysis

Managing seepage through levees requires regular maintenance and monitoring to detect and address potential issues proactively. Identifying and mitigating seepage-related problems can be challenging and costly. The study conducted an analysis of water flow through the levee of interest, considering various scenarios detailed in Chapter III. Some key findings are summarized in Table 4.1, under steady-state and rapid drawdown situations, respectively.

Table 4.1 Water flux rate under steady-state and rapid drawdown situation

Flood loading	10 H	10 F	25 H	25 F	50 H	50 F
Level of water (m)	18.33	20.46	19.54	21.38	20.54m	21.9
Steady state	4.02E-07	4.64E0-6	2.20E-06	1.67E-05	4.64E-06	2.07E-05
Rapid drawdown	4.02E-07	2.09E-06	1.60E-06	2.89E-06	2.09E-06	3.84E-06

Comparison the water flux and rapid drawdown of Elkhorn levee under steady state and rapid drawdown situation by considering different flood return period scenarios.

The results indicate that the flux rate falls within the range of laminar flow, ensuring the stability of both the dam body and foundation against hydrodynamic forces caused by seepage. Simultaneously, the rate of water loss poses no threat of inundation to adjacent land, even under the most extreme future flood conditions.

The hydraulic gradients, as presented in Table 4.2, exhibit a positive correlation with flood volume, with the highest values being associated with future floods. This suggests that flash floods, resulting from climate change, pose a considerable risk of piping and internal erosion and subsequently endanger the stability of the geo-structure. It is crucial to address and manage these risks to safeguard the integrity of the levee and protect surrounding areas from potential hazards. Noteworthy, these high values are corresponding to the clay layer that is naturally resistant to high hydraulic gradients.

Table 4.2 Hydraulic gradients under steady-state and rapid drawdown situation

Flood loading	10 H	10 F	25 H	25 F	50 H	50 F
level of water (m)	18.33	20.46	19.54	21.38	20.54	21.9
Steady-state	0.49	2.12	1.35	2.86	2.12	3.27
Rapid drawdown	0.49	1.58	1.07	1.95	1.58	2.15

Comparison the hydraulic gradients of elkhorn levee under steady-state and rapid drawdown situation by considering different flood return period scenarios.

Seepage through the levee, especially during high water levels or flood events, can increase the risk of overtopping. Overtopping can lead to erosion of the levee's crest and potential failure, resulting in flooding of adjacent areas.

Stationary Mechanical Behavior of the Levee

The mechanical response of the Elkhorn levee was analyzed under body loads, and the resulting maximum level of internal stresses and displacements are presented in Table 4.3.

Table 4.3 Maximum stress invariants and deformations under steady state situation

Flood loading	10 H	10 F	25 H	25 F	50 H	50 F
level of water (m)	18.33	20.46	19.54	21.38	20.54	21.9
Deviator stress (q)	69.89	63.39	65.22	60.95	63.39	59.66
Mean Effective Stress (p')	142.84	131.52	137.82	127.5	131.52	125.36
Displacement (x)	0.027	0.028	0.029	0.0285	0.028	0.029
Displacement (y)	0.138	0.125	0.13	0.121	0.125	0.119

Comparison the deviator stress, mean effective stress and x and y direction displacement.

Figure 4.1, shows the flood induces both vertical and horizontal deformations within the levee and its foundation. Specifically, the hydrostatic forces' horizontal components on the upstream face exert pressure, pushing the levee towards the downstream side. As the flood elevation increases, the settlement also becomes more substantial.

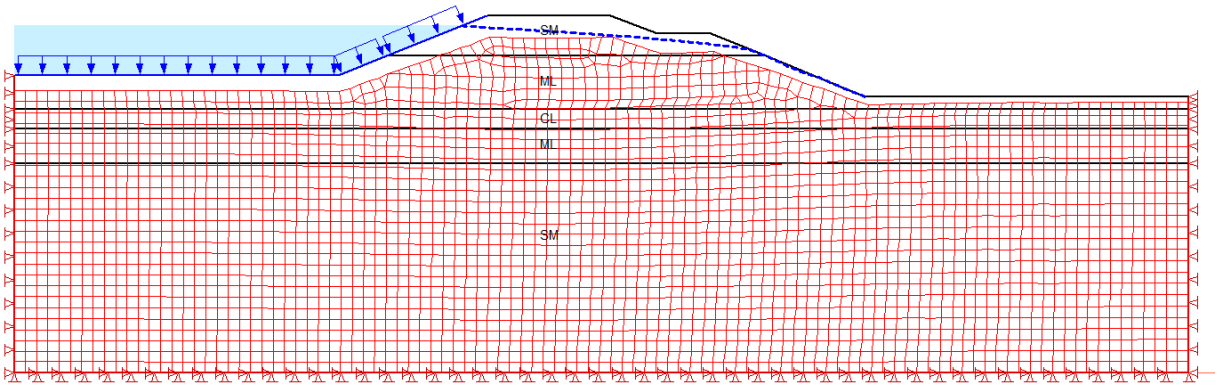

Figure 4.1 Resultant displacement shape of the levee

Table 4.4, reveals that the elastic components of deformation recover during the rapid drawdown, which implies the removing of the weight of the upstream water. This unloading process allows the levee to partially regain its original shape.

Table 4.4 Maximum stress invariants and deformations under rapid drawdown situation

Flood loading	10 H	10 F	25 H	25 F	50 H	50 F
level of water (m)	18.33	20.46	19.54	21.38	20.54m	21.9
Deviator stress (q)	69.89	60.85	65.05	60.22	60.76	60.49
Mean Effective Stress (p')	142.84	133.62	137.64	131.6	133.76	130.87
Displacement (x)	0.027	0.032	0.03	0.035	0.032	0.037
Displacement (y)	0.138	0.123	0.13	0.117	0.122	0.115

Comparison the deviator stress, mean effective stress and x and y direction displacement.

The initial stress state, including pore water pressure, mean effective stress (p'), and deviator stress (q), plays a critical role in determining the drained and undrained shear strength of each element of the parent model when performing the dynamic finite element analysis. These parameters are also utilized when assessing slope stability. Examining the Table 4.3 and Table 4.4, it is evident that the mean effective stress decreases with the water level due to the incomplete dissipation of excess pore water pressure over the transient phase and the rise in the pore water pressure attributed to the weight of the water. In contrast, the change in deviator stress is negligible, limited to only 5% of its initial value. This observation is explained by the fact that pore water pressure does not influence the deviator stress.

Static and Pseudo Dynamic Slope Stability

The levee's stability analysis is conducted under steady-state water flow and body loads, utilizing both pseudo-dynamic slope stability and static slope stability assessments. Similarly, slope stability under static and pseudo-dynamic conditions was evaluated under the transient condition of rapid drawdown. In pseudo-dynamic analyses, a horizontal constant acceleration equal to half of the desired quake acceleration, not exceeding 0.2, (USACE, 1982) is applied to the body load.

Table 4.5 The static and pseudo-dynamic analyses under steady-state situation

Flood loading	10 H	10 F	25 H	25 F	50 H	50 F
level of water (m)	18.33	20.46	19.54	21.38	20.54	21.9
Static	2.04	1.62	1.95	1.55	1.62	1.5
(0.075 g)	1.65	1.34	1.58	1.28	1.34	1.24
(0.1 g)	1.54	1.26	1.48	1.2	1.26	1.17
(0.15 g)	1.37	1.13	1.32	1.09	1.13	1.05
(0.2 g)	1.2	1.03	1.18	1.0	1.03	0.95

Comparison the factor of safety for the downstream slopes of Elkhorn levee for 24 different scenarios of flood and earthquake coincidence under steady-state situation.

The results of the static and pseudo-dynamic analyses are presented in Table 4.5 and Table 4.6, focusing on the downstream slope stability under steady-state and rapid drawdown situations, respectively.

Table 4.6 The static and pseudo-dynamic analyses under rapid drawdown situation

Flood loading	10 H	10 F	25 H	25 F	50 H	50 F
level of water (m)	18.33	20.46	19.54	21.38	20.54m	21.9
Stable state	2.04	1.48	1.78	1.3	1.48	1.2
(0.075 g)	1.65	1.16	1.43	1	1.16	0.92
(0.1 g)	1.54	1.08	1.33	0.93	1.08	0.85
(0.15 g)	1.37	0.94	1.16	0.8	0.94	0.74
(0.2 g)	1.2	0.84	1.03	0.72	0.84	0.66

Comparison the factor of safety for the downstream slopes of Elkhorn levee for 24 different scenarios of flood and earthquake coincidence under rapid drawdown situation.

It is evident that climate change, leading to larger floods, reduces safety factors under both static and pseudo-dynamic analyses when hydrostatic pressure is present as well as after rapid drawdown. Larger floods saturating a greater volume of the levee body result in higher pore water pressure and lower safety factors.

Table 4.7 and Table 4.8, displays the factor of safety for the upstream slopes under steady-state and rapid drawdown situation, respectively.

Table 4.7 The factor of safety for the upstream slopes under steady-state situation

Flood loading	10 H	10 F	25 H	25 F	50 H	50 F
level of water (m)	18.33	20.46	19.54	21.38	20.54m	21.9
Stable state	2.19	1.97	2.2	2.36	1.97	2.7
(0.075 g)	1.8	1.57	1.8	1.71	1.57	1.85
(0.1 g)	1.68	1.47	1.68	1.56	1.47	1.67
(0.15 g)	1.5	1.29	1.49	1.33	1.29	1.39
(0.2 g)	1.36	1.15	1.34	1.14	1.15	1.18

Comparison the factor of safety for the upstream slopes of Elkhorn levee for 24 different scenarios of flood and earthquake coincidence under steady-state situation.

These results indicate that the level of concern regarding the stability of the upstream slope is lower compared to the downstream one. This discrepancy in safety factors can be attributed to the contribution of the silt layer to the slip surface on each side.

Table 4.8 The factor of safety for the upstream slopes under rapid drawdown situation

Flood loading	10 H	10 F	25 H	25 F	50 H	50 F
level of water (m)	18.33	20.46	19.54	21.38	20.54m	21.9
Stable state	2.19	1.9	2	1.84	1.9	1.78
(0.075 g)	1.8	1.56	1.65	1.46	1.56	1.38
(0.1 g)	1.68	1.46	1.55	1.35	1.46	1.28
(0.15 g)	1.5	1.27	1.39	1.17	1.27	1.1
(0.2 g)	1.36	1.13	1.23	1.02	1.13	0.96

Comparison the factor of safety for the upstream slopes of Elkhorn levee for 24 different scenarios of flood and earthquake coincidence under rapid drawdown situation.

Moreover, after rapid drawdown events, safety factors are lower compared to those achieved when hydrostatic pressure is present on the upstream face of the levee. While all safety factors under steady-state conditions are above one, most of them drop below unity during the analysis after rapid drawdown, indicating instability at this condition. This behavior is attributed to water drainage and associated hydrodynamic pressures, which reduce the effective stress and shear strength.

Further, horizontal body loads (to simulate the acceleration of the earthquake) significantly reduce the factor of safety, even when these loads are relatively low. The highest percentage of reduction occurs between the static state and scenarios involving low horizontal acceleration. This suggests that even minor horizontal acceleration can considerably impact the stability of the levee which is already under hydro-dynamic loads of floods.

Liquefaction Potential

The liquefaction zone for each flood and earthquake compounding was determined using Quake/W analysis. In this section, we classified our different earthquake scenarios into four different design earthquake levels Operational Based Earthquake (OBE), Design Base Earthquake (DBE), Maximum Base Earthquake (MBE), and, Maximum Probable Earthquake (MPE). Figure 4.1, displays the areas of the levee and its foundation that experienced liquefaction under the compound of a 50-year return period flood and the MPE scenario.

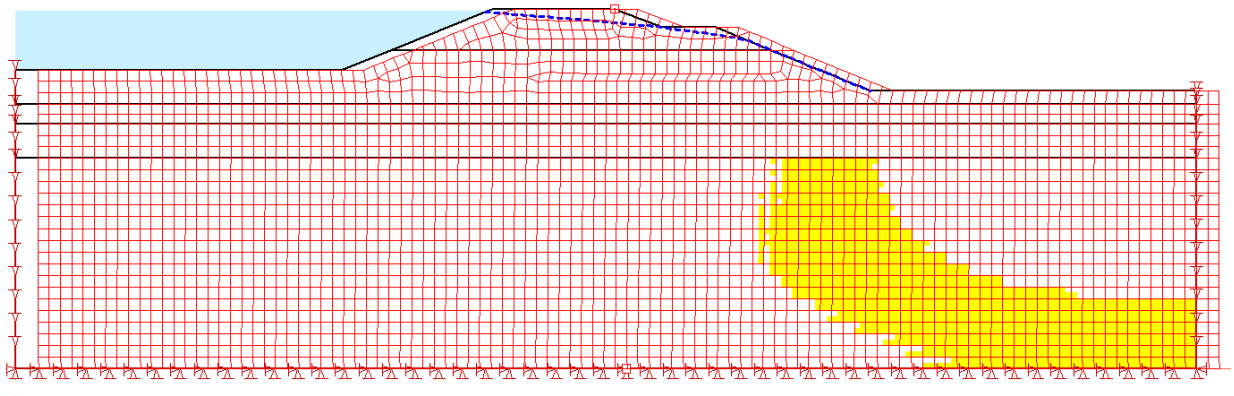

Figure 4.2 Liquefied zone under 50-year flood and MPE scenario

Table 4.9 Liquefaction potential for different scenarios under steady-state situation

Flood loading	10 H	10 F	25 H	25 F	50 H	50 F
level of water (m)	18.33	20.46	19.54	21.38	20.54m	21.9
OBE (0.15g)	N	N	N	N	N	N
DBE (0.2g)	N	N	N	N	N	N
MBE (0.3g)	Y	Y	Y	Y	Y	Y
MPE (0.5g)	Y	Y	Y	Y	Y	Y
Y: Liquefied, N: Not Liquefied						

Comparison the liquefaction potential for 24 different scenarios of flood and earthquake coincidence under steady-state situation.

The analysis reveals that the SM layer of the foundation is the only soil layer susceptible to liquefaction, primarily due to the soil plasticity or lower pore water pressure in other layers, which prevents liquefaction in the other layers. The findings are summarized in Table 4.9.

It is evident from the table that the potential for liquefaction increases with the intensity of the flood, and larger floods cause the soil medium to liquefy under lower levels of shaking. This phenomenon is attributed to higher pore water pressures that result from impoundment, creating conditions more conducive to liquefaction.

Moreover, the study indicates that liquefaction is more likely to occur in the future. Even under identical flood return periods, the soil foundation liquefies under lower levels of seismic activity. This difference is mainly driven by the higher flood levels anticipated in the future, which exacerbate the liquefaction potential.

Furthermore, the risk of liquefaction is amplified during rapid drawdown events. As demonstrated in Table 4.10, higher water levels are associated with stability against liquefaction during low to medium earthquakes. However, when rapid drawdown occurs, the soil medium liquefies under all levels of seismic activity.

Table 4.10 Liquefaction potential for different scenarios under rapid drawdown situation

Flood loading	10 H	10 F	25 H	25 F	50 H	50 F
level of water (m)	18.33	20.46	19.54	21.38	20.54m	21.9
OBE (0.15g)	N	Y	Y	Y	Y	Y
DBE (0.2g)	N	Y	Y	Y	Y	Y
MBE (0.3g)	Y	Y	Y	Y	Y	Y
MPE (0.5g)	Y	Y	Y	Y	Y	Y
Y: Liquefied, N: Not Liquefied						

Comparison the liquefaction potential for 24 different scenarios of flood and earthquake coincidence under rapid drawdown situation.

This outcome is attributed to the pressure confinement caused by the water behind the levee, leading to an increase in mean effective stress. This, in turn, moves the initial stress state further away from the failure criterion and reduces the likelihood of liquefaction.

Permanent Deformation under Earthquakes

The Newmark method was employed to assess permanent vertical deformation caused by earthquakes, and the results are presented in Table 4.11 and 4.12 under steady-state and rapid drawdown situations, respectively. The analysis indicates that settlement under DBE and OBE scenarios is negligible when storage is full, and the levee performs satisfactorily under these seismic conditions. Additionally, for all other cases, settlement remains limited to tens of centimeters while the levee is stable and subject to hydrostatic pressure.

Table 4.11 Permanent vertical deformation under steady-state situation

Flood loading	10 H	10 F	25 H	25 F	50 H	50 F
level of water (m)	18.33	20.46	19.54	21.38	20.54m	21.9
OBE (0.15g)	0	0	0	0	0	0
DBE (0.2g)	0	0	0	0.02	0	0.03
MBE (0.3g)	0	0.04	0	0.06	0.04	0.08
MPE (0.5g)	0.03	0.13	0.05	0.2	0.13	0.3

Comparison the permanent vertical deformation under steady-state situation by considering 24 different flood and earthquake coincidence scenarios.

Table 4.12 Permanent vertical deformation under rapid drawdown situation

Flood loading	10 H	10 F	25 H	25 F	50 H	50 F
level of water (m)	18.33	20.46	19.54	21.38	20.54m	21.9
OBE (0.15g)	0	0.03	0	0.12	0.03	0.3
DBE (0.2g)	0	0.09	0	0.25	0.09	0.55
MBE (0.3g)	0	0.17	0.03	0.41	0.17	0.74
MPE (0.5g)	0.03	0.43	0.14	0.9	0.43	1.46

Comparison the permanent vertical deformation under drawdown situation by considering 24 different flood and earthquake coincidence scenarios.

However, challenges arise when more intense quakes induce settlement that pushes the crest of the levee underwater. This situation leads to significant damage caused by water overtopping. Notably, the difference between the highest water level and the levee crest is a mere 10 centimeters, making cases like the 50-year return period flood (future), along with the future 25-year return period flood under MPE, susceptible to total damage due to downstream slope erosion.

The settlement of the levee under identical earthquake conditions increases with higher upstream water levels. This observation underscores the critical role played by the elevation of the phreatic line and the volume of saturated soil in influencing the dynamic response of the geo-structure. The larger the saturated volume of soil, the greater the settlement experienced.

During rapid drawdown events, earthquake-induced deformations of the studied levee become unallowable in many cases and result in a total failure of the structure. This response is attributed to the lack of support stemming from the hydro-static pressure of the water storage, the levee's saturated state, high pore water pressure, low effective stress, low shear strength, and consequently, the low factor of safety during the earthquake. The integration of accelerations, when safety factors less than one, leads to velocity calculations, and further integration yields

settlement values, which are notably larger when larger numbers of safety factors are less than unity.

Probability of Failure under Cascading Hazard

Three autonomous failure mechanisms may cause a total failure of the studied levee. The instability of up/downstream slopes could be the main cause of the levee failure which is determined via the factor of safety of less than one under either static loadings or dynamic ones. Another reason for significant damage is the excessive deformations which are accompanied by major fractures or overtopping of the water. The criterion of major fracturing was presumed settlements over 10% of the levee height. The overtopping phenomenon was determined through the assessment of the current water level and the elevation of the levee's crest after the occurrence of the settlement. Last but not least, the liquefaction of the foundation is a potential failure because that should be taken into consideration when calculating the probability of the failure. The probability of failure under cascading flood and earthquake is equal to the summation of the probabilities of the concurrent occurrence of floods and earthquakes leading to one of the abovementioned mechanisms. Hence, I highlighted the scenarios resulting in the failure based on the criteria mentioned in the previous paragraph. Subsequently, the probability of each one was determined via methods proposed by USACE (2020) and the achieved values are all added. These values are displayed in Tables [4.13 – 4.20].

Table 4.13 Probability of liquefaction under steady-state condition

Flood loading	10	25	50
OBE	0	0	0
DBE	0	0	0
MBE	2E-06	7.9E-07	4E-07
MPE	7.8E-07	3.1E-07	1.6E-07

Comparison the probability of coincidence of flood and earthquake for liquefied area under steady-state situation by considering different scenarios.

Table 4.14 Probability of liquefaction under rapid drawdown condition

Flood loading	10	25	50
OBE	1.3E-05	5.3E-06	2.7E-06
DBE	4.1E-06	1.6E-06	8.1E-07
MBE	2E-06	7.9E-07	4E-07
MPE	7.8E-07	3.1E-07	1.6E-07

Comparison the probability of coincidence of flood and earthquake for liquefied area under rapid drawdown situation by considering different scenarios.

Table 4.15 Probability of deformation under steady-state condition

Flood loading	10	25	50
OBE	0	0	0
DBE	0	0	0
MBE	0	0	0
MPE	0	0	1.6E-07

Comparison the probability of coincidence of flood and earthquake for areas that permanently deformed under rapid steady-state situation by considering different scenarios.

Table 4.16 Probability of deformation under rapid drawdown condition

Flood loading	10	25	50
OBE	0	0	0
DBE	0	0	8.1E-07
MBE	0	7.9E-07	4E-07
MPE	7.8E-07	3.1E-07	1.6E-07

Comparison the probability of coincidence of flood and earthquake for areas that permanently deformed under rapid drawdown situation by considering different scenarios.

Table 4.17 Probability of failure of the downstream side under pseudo-static loads under steady-state condition

Flood loading	10	25	50
OBE	0	0	0
DBE	0	0	0
MBE	0	0	0
MPE	0	0	1.6E-07

Comparison the probability of coincidence of flood and earthquake for downstream side of the Elkhorn levee that failed under steady-state situation by considering different scenarios.

Table 4.18 Probability of failure of the downstream side under pseudo-static loads under rapid drawdown condition

Flood loading	10	25	50
OBE	0	0	2.7E-06
DBE	0	1.6E-06	8.1E-07
MBE	2E-06	7.9E-07	4E-07
MPE	7.8E-07	3.1E-07	1.6E-07

Comparison the probability of coincidence of flood and earthquake for downstream side of the Elkhorn levee that failed under rapid drawdown situation by considering different scenarios.

Table 4.19 Probability of failure of the upstream side under pseudo-static loads under steady-state condition

Flood loading	10	25	50
OBE	0	0	0
DBE	0	0	0
MBE	0	0	0
MPE	0	0	0

Comparison the probability of coincidence of flood and earthquake for upstream side of the Elkhorn levee that failed under steady-satate situation by considering different scenarios.

Table 4.20 Probability of failure of the downstream side under pseudo-static loads under rapid drawdown condition

Flood loading	10	25	50
OBE	0	0	0
DBE	0	0	0
MBE	0	0	0
MPE	0	0	1.6E-07

Comparison the probability of coincidence of flood and earthquake for upstream side of the Elkhorn levee that failed under rapid drawdown situation by considering different scenarios.

This finding is equal to the probability of failure under compound flood and earthquake over each year of the next 50-year period and therefore, the total failure equals 50 times of the mentioned finding. Thus, the final result which denote the total probability of the failure of the Elkhorn levee under the concurrent flood and earthquake during next 50-year period is equal to 0.00183. In other words, 1.83 meters of each kilometer of the levee will be totally damaged over the next 50 years because of the cascading flood and earthquake. As the length of the levee is around 42 miles or 67 km (USACE 2019), length of the embankment damage would be more than 122.5 meters of the levee in total.

Conclusion

In this chapter, a comprehensive numerical analysis was conducted using the Geo/slope software in order to evaluate the performance of the Elkhorn levee under compound flood and earthquake loading conditions. There were several geotechnical parameters that were evaluated, which revealed that the stability of the levee is influenced by a number of factors such as flux, hydraulic gradients, mechanical behavior, and the potential for liquefaction. It has been determined that the probability of failure under cascading flood events and earthquake events, which are expected to occur over the next 50 years, is 0.00183. This means that multiple sections of the levee are likely to suffer damage. These findings provide valuable insights into enhancing the levee's

resilience and providing a practical approach to the sustainability analysis of similar multiple-hazard levee systems that can be applied to enhancing their resilience.

CHAPTER V

SUMMARY AND CONCLUSION

Summary

This study focused on the vulnerability of levees to cascading earthquakes and floods, with a particular focus on the Elkhorn Levee in Sacramento County, California. A case study of the Sacramento-San Joaquin Delta region, known for high-risk disaster potential, was selectively chosen due to its dense population, extensive levee network, and multiple factors leading to potential failure. The evaluation involves various scenarios with different flood and seismic conditions to assess the levee's response and critical geotechnical parameters. The Elkhorn Levee, a prominent levee in the region, is studied in detail with a cross-section provided for reference.

The authors presented an elaborated approach to evaluating the liquefaction zone of the Elkhorn Levee using the GeoStudio package, incorporating SLOPE/W, SEEP/W, SIGMA/W, and QUAKE/W software. The Fault Tree Method was then utilized to determine the levee's reliability, considering the probability of concurrent floods and earthquakes.

SEEP/W software was employed to model steady-state and transient flow conditions to evaluate the impact of different return periods of floods on the levee. Streamflow and flood level data are analyzed for various recurrence intervals to design resilient infrastructures.

SIGMA/W software was used to analyze the stress distribution within the soil medium, assessing its susceptibility to deformation and potential failure. Mohr-Coulomb elastic-plastic

constitutive model parameters were selected based on experimental results available in the literature.

QUAKE/W software is utilized to estimate seismic loading at the base of the levee's foundation using historical earthquake data. The study considers the probability of ground motion causing potential damage in Sacramento. The peak acceleration for different earthquake returns periods was also calculated from the seismic hazard analysis provided in the literature and inserted in the software.

The thesis also clarified the importance of elastoplastic parameters such as shear strength parameters, Poisson's ratio, and Young's modulus in soil behavior. Seed and Lee's (1965) cyclic testing on Sacramento River Sand is referenced to assess soil susceptibility based on compaction conditions. Various parameters like void ratio and confining pressure are used to estimate the shear modulus (G), $G_{\max}$, damping ratio, and cyclic stress ratio (CSR) when using QUAKE/W software.

Overall, this thesis contributes valuable insights into assessing the vulnerability of levees to simultaneous floods and earthquakes, with a focus on the Elkhorn Levee case study in the Sacramento-San Joaquin Delta region. The use of advanced software and comprehensive analysis methods enhances our understanding of soil dynamics and helps improve the design and resilience of critical infrastructure in high-risk areas. The thesis concluded with an exploration of soil susceptibility to liquefaction, slope instability, and permanent deformation under dynamic loading conditions.

Conclusion

The following conclusions are drawn from this thesis:

First of all, this study focuses on flux and hydraulic gradients to understand how floodwater and earthquake-induced vibrations affect the levee's foundation and stability. The investigation

shows that the flux rate falls within the range of laminar flow, ensuring stability against hydrodynamic forces caused by seepage. The hydraulic gradients exhibit a positive correlation with flood volume, indicating a considerable risk of piping and internal erosion during flash floods, which could endanger the levee's stability. However, the highest hydraulic gradients in the levee of interest take place within the plastic clay layer which is resistant to piping. The study also shows that the risk of overtopping is low, even under extreme future flood conditions.

The mechanical behavior analysis shows that flood-induced horizontal forces cause settlement and deformation within the levee and its foundation. During the rapid drawdown, the levee can partially regain its original shape due to unloading.

Static and pseudo-dynamic slope stability analyses under steady-state and rapid drawdown conditions show that larger floods reduce safety factors under both scenarios, making the levee more susceptible to instability. Horizontal body loads during earthquakes significantly reduce the factor of safety, indicating that even minor horizontal acceleration can impact the levee's stability under flood conditions.

The study also evaluates the potential for liquefaction under various flood and earthquake compound. The results show that the soil foundation liquefies under lower levels of shaking with higher flood levels, indicating an increased risk of liquefaction in the future due to climate change.

Permanent deformation assessment under earthquakes demonstrates that settlement increases with higher upstream water levels, which can lead to significant damages and water overtopping. During rapid drawdown, earthquake-induced deformations can lead to total failure of the levee.

In conclusion, the numerical analysis provides valuable insights into the performance of the Elkhorn levee under various flood and seismic scenarios. The findings can be used to enhance the design and management of levee systems facing similar multi-hazard challenges, improving.

REFERENCES

Abdollahi, M., & Vahedifard, F. Evaluation of Levees under Compound Flood-Earthquake Loadings. In *Geo-Extreme 2021* (pp. 69-78).

Alexander, D. (2018). *Natural disasters*. Routledge.

Arya, L. M., & Paris, J. F. (1981). A physicoempirical model to predict the soil moisture characteristic from particle-size distribution and bulk density data. *Soil Science Society of America Journal*, *45*(6), 1023-1030.

Aubertin, M., Mbonimpa, M., Bussière, B., & Chapuis, R. P. (2003). A model to predict the water retention curve from basic geotechnical properties. *Canadian Geotechnical Journal*, *40*(6), 1104-1122.

Azmoon, B., Biniyaz, A., & Liu, Z. (2021). Evaluation of deep learning against conventional limit equilibrium methods for slope stability analysis. *Applied Sciences*, *11*(13), 6060.

Budhu, M. 2010. Soil mechanics and foundations. 3rd ed. Hoboken, NJ: Wiley.

Burton, C., & Cutter, S. L. (2008). Levee failures and social vulnerability in the Sacramento-San Joaquin Delta area, California. Natural hazards review, 9(3), 136-149.

Chowdhury, K. (2023), USACE State of Practice for Seismic Evaluation of Dams and Levees. *US Army Crops of Engineers, Engineer Research & Development Center.*

Deverel, S. J., Bachand, S., Brandenberg, S. J., Jones, C. E., Stewart, J. P., & Zimmaro, P. (2016). Factors and processes affecting delta levee system vulnerability. San Francisco Estuary and Watershed Science, 14(4).

Duncan, J. M. (1996). State of the art: limit equilibrium and finite-element analysis of slopes. *Journal of Geotechnical engineering*, *122*(7), 577-596.

Duncan, J. M. (2000). Factors of safety and reliability in geotechnical engineering. *Journal of geotechnical and geoenvironmental engineering*, *126*(4), 307-316.

Duncan, J. M., Wright, S. G., & Brandon, T. L. (2014). *Soil strength and slope stability*. John Wiley & Sons.

Elhakim, A. F. (2016). Estimation of soil permeability. *Alexandria Engineering Journal*, *55*(3), 2631-2638.

Ellingwood, B.R. (1995). Event Combination Analysis for Design and Rehabilitation of U.S. Army Corps of Engineers Navigation Structures, Contract Report ITL-95-2, U.S. Army Corps of Engineers, Waterways Experiment Station, Vicksburg, MS.

Eshrati, L., Mahmoudzadeh, A., & Taghvaei, M. (2015). Multi hazards risk assessment, a new methodology. *International Journal of Health System and Disaster Management, 3*(2), 79.

Flynn, S. (2007). *The Edge of Disaster: Rebulding a Resilient Nation*. Random House.

Franczyk, A., Dwornik, M., & Leśniak, A. (2016). Numerical modelling of the impact of flood wave cyclicality on the stability of levees. In *E3S Web of Conferences* (Vol. 7, p. 03022). EDP Sciences.

Fredlund, D. G., & Scoular, R. E. G. (1999, November). Using limit equilibrium concepts in finite element slope stability analysis. In *Proceedings of the International Symposium on Slope stability Engineering-IS Shikoku* (Vol. 99, pp. 31-47).

Fredlund, D. G., & Xing, A. (1994). Equations for the soil-water characteristic curve. *Canadian geotechnical journal*, *31*(4), 521-532.

Fredlund, D. G., Morgenstern, N. R., & Widger, R. A. (1978). The shear strength of unsaturated soils. *Canadian geotechnical journal*, *15*(3), 313-321.

Fredlund, M. D., Fredlund, D. G., & Wilson, G. W. (1997, April). Prediction of the soil-water characteristic curve from grain-size distribution and volume-mass properties. In *Proc., 3rd Brazilian Symp. on Unsaturated Soils* (Vol. 1, pp. 13-23). Rio de Janeiro.

Gao, W., Watts, C. W., Ren, T., Shin, H. C., Taherzadeh, S., Attenborough, K., ... & Whalley, W. R. (2013). Estimating penetrometer resistance and matric potential from the velocities of shear and compression waves. *Soil Science Society of America Journal*, *77*(3), 721-728.

GeoStudio, (2022).” Dynamic Earthquake Modeling with GeoStudio”, Seequent Limited, The Bentley Subsurface Company. Pp.171.

Girardi, V., Ceccato, F., Rohe, A., Simonini, P., & Gabrieli, F. (2023). Failure of levees induced by toe uplift: Investigation of post-failure behavior using material point method. *Journal of Rock Mechanics and Geotechnical Engineering*, *15*(4), 970-983.

Griffiths, D. V., & Fenton, G. A. (2004). Probabilistic slope stability analysis by finite elements. *Journal of geotechnical and geoenvironmental engineering*, *130*(5), 507-518.

Gupta, S., & Larson, W. E. (1979). Estimating soil water retention characteristics from particle size distribution, organic matter percent, and bulk density. *Water resources research*, *15*(6), 1633-1635.

Haldar, A., & Tang, W. H. (1979). Probabilistic evaluation of liquefaction potential. *Journal of the Geotechnical Engineering Division*, *105*(2), 145-163.

Hanzawa, H., Itoh, Y., & Suzuki, K. (1979). Shear characteristics of a quick sand in the Arabian Gulf. *Soils and Foundations*, *19*(4), 1-15.

Hardin, B. O. (1978, June). The nature of stress-strain behavior for soils. In *From Volume I of Earthquake Engineering and Soil Dynamics--Proceedings of the ASCE Geotechnical Engineering Division Specialty Conference, June 19-21, 1978, Pasadena, California. Sponsored by Geotechnical Engineering Division of ASCE in cooperation with:* (No. Proceeding).

Hardin, B. O., & Drnevich, V. P. (1972). Shear modulus and damping in soils: design equations and curves. *Journal of the Soil mechanics and Foundations Division*, *98*(7), 667-692.

Haverkamp, R., & Parlange, J. Y. (1986). PREDICTING THE WATER-RETENTION CURVE FROM PARTICLE-SIZE DISTRIBUTION: 1. SANDY SOILS WITHOUT ORGANIC MATTER: 1. *Soil science*, *142*(6), 325-339.

Hillier, J. K., Matthews, T., Wilby, R. L., & Murphy, C. (2020). Multi-hazard dependencies can increase or decrease risk. *Nature Climate Change*, *10*(7), 595-598.

Huang, X., Stevenson, S., & Hall, A. D. (2020). Future warming and intensification of precipitation extremes: A "double whammy" leading to increasing flood risk in California. *Geophysical Research Letters*, *47*(16), e2020GL088679.

Huang, Y. H. (2014, February). Slope stability analysis by the limit equilibrium method: Fundamentals and methods. American Society of Civil Engineers.

Huang, Y., & Yu, M. (2013). Review of soil liquefaction characteristics during major earthquakes of the twenty-first century. *Natural hazards*, *65*, 2375-2384.

Inci, G., Yesiller, N., & Kagawa, T. (2003). Experimental investigation of dynamic response of compacted clayey soils. *Geotechnical Testing Journal*, *26*(2), 125.

Ishibashi, I., & Zhang, X. (1993). Unified dynamic shear moduli and damping ratios of sand and clay. *Soils and foundations*, *33*(1), 182-191.

Ishihara, K. (1993). Liquefaction and flow failure during earthquakes. *Geotechnique*, *43*(3), 351-451.

Jefferies, M., & Been, K. (2015). *Soil liquefaction: a critical state approach*. CRC press.

Jibson, R. W. (1993). Predicting earthquake-induced landslide displacements using Newmark's sliding block analysis. *Transportation research record*, *1411*, 9-17.

Kappes, M. S., Keiler, M., von Elverfeldt, K., & Glade, T. (2012). Challenges of analyzing multi-hazard risk: a review. *Natural hazards*, *64*, 1925-1958.

Kaur, A., & Sharma, R. K. (2016). Slope stability analysis techniques: A review. *International Journal of Engineering Applied Sciences and Technology*, *1*(4), 52-57.

Khabbaz, H., Fatahi, B., & Nucifora, C. (2012). Finite element methods against limit equilibrium approaches for slope stability analysis. In *Australia New Zealand Conference on Geomechanics*. Geomechanical Society and New Zealand Geotechnical Society.

Khalili, N., & Khabbaz, M. H. (1998). A unique relationship for χ for the determination of the shear strength of unsaturated soils. *Geotechnique*, *48*(5), 681-687.

Khalilzad, M., Gabr, M. A., & Hynes, M. E. (2014). Effects of woody vegetation on seepage-induced deformation and related limit state analysis of levees. *International Journal of Geomechanics*, *14*(2), 302-312.

Kim, J., Hwang, W., & Kim, Y. (2018). Effects of hysteresis on hydro-mechanical behavior of unsaturated soil. *Engineering Geology*, *245*, 1-9.

Kumar Thota, S., Duc Cao, T., & Vahedifard, F. (2021). Poisson's ratio characteristic curve of unsaturated soils. *Journal of Geotechnical and Geoenvironmental Engineering*, *147*(1), 04020149.

Kundzewicz, Z. W. (1999). Flood protection—sustainability issues. Hydrological Sciences Journal, 44(4), 559-571.

Lee, W. S., Grosh, D. L., Tillman, F. A., & Lie, C. H. (1985). Fault tree analysis, methods, and applications ☐ a review. *IEEE transactions on reliability*, *34*(3), 194-203.

Leong, E. C., & Rahardjo, H. (1997). Review of soil-water characteristic curve equations. *Journal of geotechnical and geoenvironmental engineering*, *123*(12), 1106-1117.

Likos, W. J., & Lu, N. (2004). Hysteresis of capillary stress in unsaturated granular soil. *Journal of Engineering mechanics*, *130*(6), 646-655.

Liu, S. Y., Shao, L. T., & Li, H. J. (2015). Slope stability analysis using the limit equilibrium method and two finite element methods. *Computers and Geotechnics*, *63*, 291-298.

Mallakpour, I., Sadegh, M., & AghaKouchak, A. (2020). Changes in the exposure of California's levee-protected critical infrastructure to flooding hazard in a warming climate. *Environmental Research Letters*, *15*(6), 064032.

Mayne, P. W., & Rix, G. J. (1993). -Relationships for Clays. *Geotechnical Testing Journal*, *16*(1), 54-60.

Mualem, Y. (1986). Hydraulic conductivity of unsaturated soils: prediction and formulas. *Methods of Soil Analysis: Part 1 Physical and Mineralogical Methods*, *5*, 799-823.

Obermeier, S. F., Olson, S. M., & Green, R. A. (2005). Field occurrences of liquefaction-induced features: a primer for engineering geologic analysis of paleoseismic shaking. *Engineering Geology*, *76*(3-4), 209-234.

Oh, W. T., & Vanapalli, S. K. (2018). Modeling the stress versus settlement behavior of shallow foundations in unsaturated cohesive soils extending the modified total stress approach. *Soils and foundations*, *58*(2), 382-397.

Pasternack, S. C., & Gao, S. (1988). Numerical methods in the stability analysis of slopes. *Computers & Structures*, *30*(3), 573-579.

Perera, Y. Y., Zapata, C. E., Houston, W. N., & Houston, S. L. (2005). Prediction of the soil-water characteristic curve based on grain-size-distribution and index properties. In *Advances in pavement engineering* (pp. 1-12).

Perucca, L. P., & Moreiras, S. M. (2006). Liquefaction phenomena associated with historical earthquakes in San Juan and Mendoza Provinces, Argentina. *Quaternary International*, *158*(1), 96-109.

Poulos, S. J., Castro, G., & France, J. W. (1985). Liquefaction evaluation procedure. *Journal of Geotechnical Engineering*, *111*(6), 772-792.

Quinn, M. C., & Taylor, O. D. S. (2014). Hazard topography: visual approach for identifying critical failure combinations for infrastructure. *Natural Hazards Review*, *15*(4), 04014012.

Rahardjo, H., Fredlund, M. D., & Fredlund, D. G. (2012). Unsaturated soil mechanics in engineering practice.

Robinson, J. D., & Vahedifard, F. (2016). Weakening mechanisms imposed on California's levees under multiyear extreme drought. Climatic change, 137(1-2), 1-14.

Salem, H. S. (2000). Poisson's ratio and the porosity of surface soils and shallow sediments, determined from seismic compressional and shear wave velocities. *Geotechnique*, *50*(4), 461-463.

Salunkhe, D. P., Bartakke, R. N., Chvan, G., & Kothavale, P. R. (2017). An overview on methods for slope stability analysis. *International Journal of Engineering Research & Technology (IJERT)*, *6*(03), 2278-0181.

Seed, H. B., & Idriss, I. M. (1971). Simplified procedure for evaluating soil liquefaction potential. *Journal of the Soil Mechanics and Foundations division*, *97*(9), 1249-1273.

Selmi, M., Hamdi, Y., & Moiriat, D. (2022). Multi-Hazard Assessment of a Flood Protection Levee. *Atmosphere*, *13*(10), 1741.

Sladen, J. A., D'hollander, R. D., & Krahn, J. (1985). The liquefaction of sands, a collapse surface approach. *Canadian geotechnical journal*, *22*(4), 564-578.

Suwal, L. P., & Kuwano, R. (2013). Disk shaped piezo-ceramic transducer for P and S wave measurement in a laboratory soil specimen. *Soils and foundations*, *53*(4), 510-524.

Swain, D. L., Wing, O. E., Bates, P. D., Done, J. M., Johnson, K. A., & Cameron, D. R. (2020). Increased flood exposure due to climate change and population growth in the United States. *Earth's Future*, *8*(11), e2020EF001778.

Toppozada, T., & Branum, D. (2004). California earthquake history. *Annals of Geophysics*.

Toprak, S., & Holzer, T. L. (2003). Liquefaction potential index: field assessment. *Journal of Geotechnical and Geoenvironmental Engineering*, *129*(4), 315-322.

Tracy, F. T., Brandon, T. L., & Corcoran, M. K. (2016). Transient seepage analyses in levee engineering practice.

Tyagunov, S., Vorogushyn, S., Muñoz Jimenez, C., Parolai, S., & Fleming, K. (2018). Multi-hazard fragility analysis for fluvial dikes in earthquake-and flood-prone areas. *Natural hazards and earth system sciences*, *18*(9), 2345-2354.

Vahedifard, F, Jasim, F. H., Tracy, F. T., Abdollahi, M., Alborzi, A., and AghaKouchak, A. (2020). Levee fragility behavior under projected future flooding in a warming climate. Journal of J. Geotech. Geoenviron. En., 146 (12), 04020139.

Vaid, Y. P., & Chern, J. C. (1983). Effect of static shear on resistance to liquefaction. *Soils and foundations*, *23*(1), 47-60.

Van Genuchten, M. T. (1980). A closed-form equation for predicting the hydraulic conductivity of unsaturated soils. *Soil science society of America journal*, *44*(5), 892-898.

Vanapalli, S. K., & Fredlund, D. G. (1999, August). Empirical procedures to predict the shear strength of unsaturated soils. In *Eleventh Asian regional conference on soil mechanics and geotechnical engineering* (pp. 93-96).

Vanapalli, S. K., Fredlund, D. G., Pufahl, D. E., & Clifton, A. W. (1996). Model for the prediction of shear strength with respect to soil suction. *Canadian geotechnical journal*, *33*(3), 379-392.

Velea, D., Shields, F. D., & Sabatier, J. M. (2000). Elastic wave velocities in partially saturated Ottawa sand: Experimental results and modeling. *Soil Science Society of America Journal*, *64*(4), 1226-1234.

Walshire, L. A., & Robbins, B. A. (2017). SWCC prediction: Seep/W add-In functions.

Wang, J., He, Z., & Weng, W. (2020). A review of the research into the relations between hazards in multi-hazard risk analysis. *Natural Hazards*, *104*, 2003-2026.

Wang, S., Fu, J., Zhang, C., & Yang, J. (2021). *Shield Tunnel Engineering: From Theory to Practice*. Elsevier.

Wright, D. B., Bosma, C. D., & Lopez-Cantu, T. (2019). US hydrologic design standards insufficient due to large increases in the frequency of rainfall extremes. *Geophysical Research Letters*, *46*(14), 8144-8153.

Wu, Q., Li, D. Q., Liu, Y., & Du, W. (2021). Seismic performance of earth dams founded on liquefiable soil layer subjected to near-fault pulse-like ground motions. *Soil Dynamics and Earthquake Engineering*, *143*, 106623.

Yang, H., Rahardjo, H., Leong, E. C., & Fredlund, D. G. (2004). A study of infiltration on three sand capillary barriers. *Canadian Geotechnical Journal*, *41*(4), 629-643.

Yang, Q., Zhu, B., & Hiraishi, T. (2021). Probabilistic evaluation of the seismic stability of infinite submarine slopes integrating the enhanced Newmark method and random field. *Bulletin of Engineering Geology and the Environment*, *80*, 2025-2043.

Yegian, M. K., & Whitman, R. V. (1978). Risk analysis for ground failure by liquefaction. *Journal of the Geotechnical Engineering Division*, *104*(7), 921-938.

Zhai, Q., Rahardjo, H., Satyanaga, A., Zhu, Y., Dai, G., & Zhao, X. (2021). Estimation of wetting hydraulic conductivity function for unsaturated sandy soil. *Engineering Geology*, *285*, 106034.

Zhang, C., & Lu, N. (2019). Unitary definition of matric suction. *Journal of Geotechnical and Geoenvironmental Engineering*, *145*(2), 02818004.

Zhang, L. L., Zhang, J., Zhang, L. M., & Tang, W. H. (2011). Stability analysis of rainfall-induced slope failure: a review. *Proceedings of the Institution of Civil Engineers-Geotechnical Engineering*, *164*(5), 299-316.

Zhang, L., Zhan, W., & Wang, L. (2023). Probabilistic seismic analyses of earthen levees with finite element modeling. *Marine Georesources & Geotechnology*, 1-8.

Zimmaro, P., Stewart, J. P., Brandenberg, S. J., Kwak, D. Y., & Jongejan, R. (2019). Multi-hazard system reliability of flood control levees. *Soil Dynamics and Earthquake Engineering*, *124*, 345-353.

Zimmaro, P., Stewart, J. P., Brandenberg, S. J., Kwak, D. Y., & Jongejan, R. (2019). Multi-hazard system reliability of flood control levees. *Soil Dynamics and Earthquake Engineering*, *124*, 345-353.